TABLE S1. WRANGEL ISLAND AND COASTAL CHUKOTKA SAMPLE LOCATIONS

Apatite Fission Track Sample Locations (Wrangel Island)

Sample Number	*Latitude (N)*	*Longitude (E)*	*Mineral*
ELM06 WR-1A	71.0763710	-179.245505	apatite
ELM06 WR-2	71.076611	-179.245265	apatite
ELM06 WR-7B	71.03723	-179.2068	apatite
ELM06 WR-8	71.02547	-179.20808	apatite
ELM06 WR-9	71.016764	-179.198582	apatite
ELM06 WR-10B	71.09723	-179.242516	apatite
ELM06 WR-11B	71.093277	-179.244401	apatite

40Ar/39Ar Sample Locations (Wrangel Island)

ELM06 WR 11B	71.093277	-179.244401	muscovite, K-feldspar
ELM06 WR 28B	71.112346	-179.385253	muscovite
CGS C145703	71.086646	-179.233748	muscovite

40Ar/39Ar Sample Locations (Velitkenay)

EG 11B	69.184725	177.214669	hornblende
EG 15	69.185379	177.22468	biotite
EG 24	69.24786	177.31857	biotite
EG 33A	69.25338	176.94226	biotite, hornblende
EG 35A	69.26353	177.04094	biotite

U/Pb Sample Locations (Velitkenay)

VE 6	69.009522	175.311225	zircon
VE 6-7	69.009522	175.311225	zircon
VE 30	69.177974	177.155513	zircon
VE 29	69.177974	177.155513	zircon
EG 6	69.006861	175.193257	zircon
EG 8	69.172093	175.81723	zircon
EG 11A	69.184725	177.214669	zircon
EG15	69.185379	177.22468	zircon
EG 30	69.165483	177.262823	zircon
EG 31	69.224268	177.152401	zircon
EG 33A	69.25338	176.94226	zircon
EG35A	69.26353	177.04094	zircon (unpolished surfaces)

Structure samples and thin-section photomicrographs (Wrangel Island) imaged

ELM06 WR-5	71.07932	-179.249189
ELM06 WR-7C	71.03723	-179.2068
ELM06 WR-15	71.051121	-179.212657
ELM06 WR-23	71.101867	-179.477661
ELM06 WR-24	71.112134	-179.478633
ELM06 WR-28B,D	71.112346	-179.385252
ELM06 WR-39	71.117872	-179.909278
ELM06 WR-40	71.104831	-179.639861
ELM06 WR-41	71.104831	-179.639861

Table S2. Results of SHRIMP-RG zircon U-Pb dating

Sample VE6, rhyolite lower unit; 175.3075 E, 68.9793 N

Spot	% $^{206}Pb_c$	ppm U	ppm Th	$^{232}Th/^{238}U$	ppm $^{206}Pb^*$	(1) $^{206}Pb/^{238}U$ Age	(2) $^{206}Pb/^{238}U$ Age	Total $^{238}U/^{206}Pb$	±	Total $^{207}Pb/^{206}Pb$	±	(1) $^{238}U/^{206}Pb^*$	±	(1) $^{207}Pb^*/^{206}Pb^*$	±	(1) $^{207}Pb^*/^{235}U$	±	(1) $^{206}Pb^*/^{238}U$	±	err corr
VE6-3.1	0.28	252	93	0.38	2.89	85.14 ±0.9	85.19 ±0.9	74.96	1.0	0.050	4.2	75.22	1.0	0.0472	5.4	0.0865	5.5	0.01330	1	.188
VE6-8.1	0.30	161	83	0.54	1.86	85.6 ±1.1	85.9 ±1	74.28	1.2	0.050	5.1	74.85	1.3	0.0441	11	0.0812	11	0.01336	1.3	.118
VE6-6.2	0.22	451	248	0.57	5.25	86.27 ±0.8	86.64 ±0.7	73.74	0.85	0.050	3.1	74.24	0.91	0.0441	7.1	0.0819	7.1	0.01347	0.91	.127
VE6-4.1	--	80	42	0.53	0.94	87 ±1.3	87.1 ±1.4	73.6	1.6	0.047	7.8	73.60	1.6	0.0465	7.8	0.0872	7.9	0.01359	1.6	.196
VE6-5.1	--	159	63	0.41	1.87	87.9 ±1.1	87.9 ±1.1	72.86	1.2	0.047	5.3	72.86	1.2	0.0474	5.3	0.0897	5.5	0.01373	1.2	.220
VE6-1.2	--	581	198	0.35	6.92	88.56 ±0.7	88.82 ±0.7	72.15	0.8	0.047	2.8	72.30	0.8	0.0454	3.4	0.0865	3.5	0.01383	0.8	.228
VE6-7.1	--	120	44	0.38	1.44	88.6 ±1.2	89.3 ±1.2	71.97	1.3	0.045	6.2	72.31	1.3	0.0410	9.1	0.0782	9.2	0.01383	1.3	.147
VE6-2.1	0.24	98	52	0.55	1.19	89 ±1.7	90.7 ±1.6	70.4	1.7	0.050	6.7	72.00	1.9	0.0321	27	0.0610	27	0.01391	1.9	.071
VE6-6.1	0.15	859	467	0.56	10.6	92.17 ±0.7	91.98 ±0.7	69.48	0.78	0.049	2.8	69.44	0.79	0.0495	2.8	0.0983	2.9	0.01440	0.79	.269

Sample VE6-7, rhyolite upper unit; 175.3073 E, 68.9642 N

Spot	% $^{206}Pb_c$	ppm U	ppm Th	$^{232}Th/^{238}U$	ppm $^{206}Pb^*$	(1) $^{206}Pb/^{238}U$ Age	(2) $^{206}Pb/^{238}U$ Age	Total $^{238}U/^{206}Pb$	±	Total $^{207}Pb/^{206}Pb$	±	(1) $^{238}U/^{206}Pb^*$	±	(1) $^{207}Pb^*/^{206}Pb^*$	±	(1) $^{207}Pb^*/^{235}U$	±	(1) $^{206}Pb^*/^{238}U$	±	err corr
VE6_7-5.1	--	78	31	0.41	0.90	87.8 ± 2.1	86.2 ±1.8	74.7	2.1	0.0437	7.9	72.90	2.4	0.0630	18	0.1190	18	0.01371	2.4	.138
VE6_7-8.1	0.07	485	290	0.62	5.66	86.35 ± 0.78	86.9 ±0.7	73.63	0.8	0.0483	3	74.17	0.91	0.0424	7.8	0.0789	7.9	0.01348	0.91	.116
VE6_7-9.1	0.04	223	132	0.61	2.60	86 ± 1	86.98 ±1	73.58	1.1	0.0481	4.5	74.46	1.2	0.0386	13	0.0715	13	0.01343	1.2	.091
VE6_7-7.1	0.39	320	199	0.64	3.75	87.01 ± 10	87.1 ±1	73.19	1.1	0.0509	3.6	73.60	1.2	0.0465	5.9	0.0871	6	0.01359	1.2	.193
VE6_7-2.1	--	600	226	0.39	7.26	89.7 ± 0.8	90.2 ±0.8	71.02	0.9	0.0472	2.7	71.38	0.93	0.0432	4.8	0.0834	4.9	0.01401	0.93	.190
VE6_7-3.1	--	78	38	0.51	0.94	87.5 ± 2.1	90.5 ±1.9	70.8	2.0	0.0476	9.1	73.20	2.5	0.0200	64	0.0370	64	0.01367	2.5	.039
VE6_7-4.1	--	132	39	0.31	1.60	89.8 ± 1.5	90.7 ±1.5	71.2	1.6	0.0412	6.4	71.30	1.6	0.0395	7.9	0.0763	8.1	0.01402	1.6	.203
VE6_7-6.1	0.08	246	127	0.53	3.03	91.5 ± 1.1	91.7 ±1.1	69.72	1.2	0.0485	4.1	69.98	1.2	0.0456	5.4	0.0899	5.5	0.01429	1.2	.222
VE6_7-1.1	0.05	308	190	0.64	15.10	358.3 ± 2.9	358.6 ±3	17.47	0.8	0.0541	1.8	17.49	0.83	0.0530	2.1	0.4180	2.2	0.05716	0.83	.374

Sample VE30, dacitic vitrophyre, lower unit; 177.1411 E, 69.1722 N

Spot	% $^{206}Pb_c$	ppm U	ppm Th	$^{232}Th/^{238}U$	ppm $^{206}Pb^*$	(1) $^{206}Pb/^{238}U$ Age	(2) $^{206}Pb/^{238}U$ Age	Total $^{238}U/^{206}Pb$	±	Total $^{207}Pb/^{206}Pb$	±	(1) $^{238}U/^{206}Pb^*$	±	(1) $^{207}Pb^*/^{206}Pb^*$	±	(1) $^{207}Pb^*/^{235}U$	±	(1) $^{206}Pb^*/^{238}U$	±	err corr
VE30-2.2	0.54	177	60	0.35	2.08	87.64 ±0.99	87.2 ±1	73.05	1.1	0.052	4.7	73.05	1.1	0.052	4.7	0.0982	4.9	0.01369	1.1	.233
VE30-1.2	0.70	234	89	0.39	2.77	86.2 ±1.1	87.62 ±1	72.57	1.0	0.0533	5.5	74.33	1.3	0.0342	22	0.064	22	0.01346	1.3	.060
VE30-2.1	0.16	146	58	0.41	1.72	87.5 ±1.2	88.1 ±1.1	72.59	1.2	0.049	5.3	73.17	1.3	0.0426	12	0.0803	12	0.01367	1.3	.113
VE30-3.1	0.08	429	122	0.30	5.07	87.96 ±0.8	88.17 ±0.8	72.56	0.9	0.0484	3.1	72.79	0.92	0.0459	4.2	0.0869	4.3	0.01374	0.92	.213
VE30-4.1	--	593	172	0.30	7.17	89.85 ±0.71	90.03 ±0.7	71.13	0.8	0.0475	4	71.25	0.79	0.0462	4.5	0.0895	4.6	0.01404	0.79	.174

Sample VE29, rhyodacite, middle unit; 177.1489 E, 69.1700 N

Spot	% $^{206}Pb_c$	ppm U	ppm Th	$^{232}Th/^{238}U$	ppm $^{206}Pb^*$	(1) $^{206}Pb/^{238}U$ Age	(2) $^{206}Pb/^{238}U$ Age	Total $^{238}U/^{206}Pb$	±	Total $^{207}Pb/^{206}Pb$	±	(1) $^{238}U/^{206}Pb^*$	±	(1) $^{207}Pb^*/^{206}Pb^*$	±	(1) $^{207}Pb^*/^{235}U$	±	(1) $^{206}Pb^*/^{238}U$	±	err corr
VE29-2.1	0.64	323	151	0.48	3.71	84.9 ±1.4	85.3 ±1.4	74.6	1.6	0.0528	3.6	75.4	1.6	0.0443	9.1	0.0809	9.2	0.01326	1.6	.177
VE29-4.1	0.02	269	157	0.61	3.10	84.79 ±1	85.91 ±0.9	74.53	1.0	0.0479	4	75.56	1.2	0.0368	15	0.0673	15	0.01324	1.2	.079
VE29-1.1	--	453	342	0.78	5.36	87.82 ±0.8	88.28 ±0.8	72.72	0.9	0.0456	3.3	72.91	0.95	0.0436	4.1	0.0824	4.2	0.01372	0.95	.228
VE29-5.1	0.19	283	158	0.58	3.46	90.93 ±0.9	90.94 ±0.9	70.26	1.0	0.0493	4.2	70.4	0.99	0.0477	4.9	0.0935	5	0.01421	0.99	.197
VE29-3.1	--	215	193	0.93	2.65	92.5 ±1	92.3 ±1	69.63	1.1	0.045	4.7	69.18	1.1	0.05	7.7	0.0997	7.8	0.01445	1.1	.146

Sample EG6, biotite monzogranite; 175.193257 E, 69.006861 N

Spot	% $^{206}Pb_c$	ppm U	ppm Th	$^{232}Th/^{238}U$	ppm $^{206}Pb^*$	(1) $^{206}Pb/^{238}U$ Age	(2) $^{206}Pb/^{238}U$ Age	Total $^{238}U/^{206}Pb$	±	Total $^{207}Pb/^{206}Pb$	±	(1) $^{238}U/^{206}Pb^*$	±	(1) $^{207}Pb^*/^{206}Pb^*$	±	(1) $^{207}Pb^*/^{235}U$	±	(1) $^{206}Pb^*/^{238}U$	±	err corr
11EGC6-1	0.44	1057	286	0.28	15.35	107.5 ± 2.8	108.1 ± 2.8	58.90	2.6	0.0517	3.9	59.44	2.6	0.0444	6.0	0.1029	6.5	0.0168	2.6	0.404
11EGC6-2	12.55	724	848	1.21	9.29	96.0 ± 3.7	95.6 ± 3.7	58.51	3.8	0.1476	2.3	66.68	3.9	0.0506	16.8	0.1047	17.2	0.0150	3.9	0.228
11EGC6-3	0.92	2182	540	0.26	31.83	108.5 ± 2.8	108.5 ± 2.9	58.36	2.6	0.0555	1.1	58.91	2.6	0.0481	2.7	0.1127	3.8	0.0170	2.6	0.704
11EGC6-5	0.91	557	351	0.65	7.98	107.1 ± 3.7	106.7 ± 3.7	59.35	3.4	0.0554	2.5	59.71	3.5	0.0507	7.3	0.1171	8.0	0.0167	3.5	0.432
11EGC6-6	--	1434	579	0.42	21.55	111.4 ± 2.3	111.8 ± 2.3	57.26	2.0	0.0470	1.8	57.36	2.0	0.0456	2.7	0.1095	3.4	0.0174	2.0	0.606
11EGC6-7	--	677	415	0.63	9.89	109.1 ± 2.9	108.7 ± 2.9	58.87	2.7	0.0476	2.3	58.57	2.7	0.0517	3.3	0.1217	4.3	0.0171	2.7	0.631
11EGC6-8	--	381	220	0.60	5.54	107.8 ± 2.4	108.2 ± 2.4	59.34	2.2	0.0448	2.7	59.27	2.2	0.0458	4.6	0.1065	5.1	0.0169	2.2	0.439
11EGC6-9	9.74	1454	1323	0.94	20.41	103.5 ± 2.0	104.5 ± 3.8	55.23	1.8	0.1255	18	61.78	1.9	0.0405	62.8	0.0904	62.9	0.0162	1.9	0.030
11EGC6-10	0.09	970	904	0.96	13.90	106.8 ± 2.1	106.6 ± 2.1	59.89	2.0	0.0489	3.8	59.88	2.0	0.0491	4.5	0.1130	4.9	0.0167	2.0	0.409
11EGC6-11	0.81	2087	2901	1.44	28.65	102.2 ± 2.8	102.2 ± 2.8	62.09	2.7	0.0545	4.1	62.57	2.7	0.0484	5.0	0.1067	5.7	0.0160	2.7	0.481

Sample EG8, granodiorite; 175.81723 E, 69.172093 N

Spot	% $^{206}Pb_c$	ppm U	ppm Th	$^{232}Th/^{238}U$	ppm $^{206}Pb^*$	(1) $^{206}Pb/^{238}U$ Age	(2) $^{206}Pb/^{238}U$ Age	Total $^{238}U/^{206}Pb$	±	Total $^{207}Pb/^{206}Pb$	±	(1) $^{238}U/^{206}Pb^*$	±	(1) $^{207}Pb^*/^{206}Pb^*$	±	(1) $^{207}Pb^*/^{235}U$	±	(1) $^{206}Pb^*/^{238}U$	±	err corr
11EGC8-1	0.638	2037	1064	0.54	28.06	102.8 ± 2.8	102.6 ± 2.8	61.95	2.8	0.0532	1.0	62.22	2.8	0.0498	1.7	0.1103	3.3	0.0161	2.8	0.848
11EGC8-2	0.279	649	165	0.26	9.05	103.8 ± 2.5	103.7 ± 2.5	61.47	2.4	0.0503	3.2	61.60	2.4	0.0487	4.2	0.1091	4.8	0.0162	2.4	0.496
11EGC8-3	--	284	172	0.63	3.89	101.6 ± 1.8	101.9 ± 1.8	62.80	1.7	0.0479	2.9	62.95	1.8	0.0459	7.2	0.1006	7.4	0.0159	1.8	0.239
11EGC8-4	0.055	1788	553	0.32	25.21	104.9 ± 2.5	104.9 ± 2.5	60.90	2.4	0.0486	2.5	60.95	2.4	0.0479	2.9	0.1084	3.8	0.0164	2.4	0.631
11EGC8-5	--	1491	406	0.28	21.50	107.3 ± 2.0	107.3 ± 2.0	59.59	1.9	0.0478	1.3	59.58	1.9	0.0479	1.6	0.1109	2.5	0.0168	1.9	0.762
11EGC8-6	8.301	991	289	0.30	13.28	101.0 ± 3.4	99.8 ± 3.3	58.79	3.3	0.1140	1.1	63.32	3.4	0.0579	6.9	0.1260	7.7	0.0158	3.4	0.441
11EGC8-7	7.828	3797	2061	0.56	53.96	105.9 ± 2.0	105.8 ± 2.0	55.72	1.9	0.1103	1.8	60.35	1.9	0.0495	6.2	0.1131	6.5	0.0166	1.9	0.297
11EGC8-8	0.642	4065	3447	0.88	58.77	107.7 ± 2.2	107.6 ± 2.2	59.04	2.1	0.0533	3.1	59.37	2.1	0.0489	3.5	0.1135	4.1	0.0168	2.1	0.509

Sample EG33A, quartz monzodiorite; 176.942264 E, 69.253383 N

Spot	% $^{206}Pb_c$	ppm U	ppm Th	$^{232}Th/^{238}U$	ppm $^{206}Pb^*$	(1) $^{206}Pb/^{238}U$ Age	(2) $^{206}Pb/^{238}U$ Age	Total $^{238}U/^{206}Pb$	±	Total $^{207}Pb/^{206}Pb$	±	(1) $^{238}U/^{206}Pb^*$	±	(1) $^{207}Pb^*/^{206}Pb^*$	±	(1) $^{207}Pb^*/^{235}U$	±	(1) $^{206}Pb^*/^{238}U$	±	err corr
11EGC33A-1	0.049	1842	698	0.39	26.44	106.8 ± 2.3	106.8 ± 2.3	59.81	2.1	0.0486	1.3	59.84	2.1	0.0481	1.8	0.1109	2.8	0.0167	2.1	0.769
11EGC33A-2	0.081	1894	809	0.44	27.00	106.1 ± 2.6	106.1 ± 2.6	60.20	2.5	0.0488	1.2	60.24	2.5	0.0483	1.6	0.1105	2.9	0.0166	2.5	0.841
11EGC33A-3	--	1108	386	0.36	15.86	106.5 ± 2.4	106.5 ± 2.4	60.06	2.3	0.0478	1.8	60.05	2.3	0.0479	3.0	0.1101	3.8	0.0167	2.3	0.606
11EGC33A-4	0.047	1448	626	0.45	20.31	104.4 ± 2.7	104.4 ± 2.7	61.21	2.6	0.0485	1.3	61.24	2.6	0.0480	1.9	0.1082	3.3	0.0163	2.6	0.807
11EGC33A-5	0.206	1309	326	0.26	18.57	105.5 ± 2.3	105.6 ± 2.3	60.41	2.2	0.0498	1.4	60.62	2.2	0.0470	2.7	0.1070	3.5	0.0165	2.2	0.634
11EGC33A-6	0.016	1641	458	0.29	23.54	106.9 ± 2.5	106.8 ± 2.5	59.86	2.4	0.0483	1.3	59.82	2.4	0.0487	1.7	0.1123	2.9	0.0167	2.4	0.804
11EGC33A-7	0.133	753	211	0.29	10.52	104.1 ± 2.3	104.0 ± 2.3	61.40	2.2	0.0492	2.0	61.42	2.2	0.0489	3.3	0.1098	4.0	0.0163	2.2	0.554
11EGC33A-8	--	1253	247	0.20	17.89	106.4 ± 2.4	106.3 ± 2.4	60.18	2.2	0.0478	2.6	60.10	2.2	0.0489	3.1	0.1122	3.8	0.0166	2.2	0.584
11EGC33A-9	0.262	1024	450	0.45	14.52	105.8 ± 2.3	105.5 ± 2.3	60.43	2.2	0.0502	1.6	60.42	2.2	0.0503	2.3	0.1149	3.1	0.0166	2.2	0.692
11EGC33A-10	0.088	1237	425	0.36	17.20	103.3 ± 2.2	103.5 ± 2.2	61.72	2.2	0.0488	1.6	61.88	2.2	0.0468	2.9	0.1042	3.6	0.0162	2.2	0.602
11EGC33A-11	--	1001	342	0.35	14.47	107.3 ± 2.4	107.6 ± 2.4	59.49	2.2	0.0471	1.8	59.60	2.2	0.0457	3.0	0.1058	3.7	0.0168	2.2	0.601
11EGC33A-12	0.085	1404	426	0.31	20.40	108.0 ± 2.2	108.2 ± 2.3	59.05	2.1	0.0489	1.5	59.19	2.1	0.0470	2.3	0.1094	3.1	0.0169	2.1	0.679

Sample EG30, deformed leucogranite; 177.262823 E, 69.165483 N

Spot	% $^{206}Pb_c$	ppm U	ppm Th	$^{232}Th/^{238}U$	ppm $^{206}Pb^*$	(1) $^{206}Pb/^{238}U$ Age	(2) $^{206}Pb/^{238}U$ Age	Total $^{238}U/^{206}Pb$	±	Total $^{207}Pb/^{206}Pb$	±	(1) $^{238}U/^{206}Pb^*$	±	(1) $^{207}Pb^*/^{206}Pb^*$	±	(1) $^{207}Pb^*/^{235}U$	±	(1) $^{206}Pb^*/^{238}U$	±	err corr
11EGC30-11.1	0.033	1123	464	0.43	15.22	100.8 ± 1.6	100.9 ± 1.6	63.37	1.6	0.0483	1.5	63.44	1.6	0.0474	1.9	0.1029	2.5	0.0158	1.6	0.644
11EGC30-12.1	--	1581	707	0.46	21.43	100.9 ± 2.0	100.9 ± 2.0	63.40	2.0	0.0476	1.2	63.36	2.0	0.0480	1.4	0.1046	2.5	0.0158	2.0	0.828
11EGC30-21.1	0.129	838	104	0.13	11.44	101.1 ± 1.7	101.7 ± 1.7	62.83	1.7	0.0491	1.6	63.26	1.7	0.0437	3.9	0.0952	4.3	0.0158	1.7	0.394
11EGC30-1.1	0.077	1482	469	0.33	20.26	101.9 ± 3.7	101.8 ± 3.7	62.79	3.6	0.0487	2.4	62.79	3.6	0.0487	2.4	0.1069	4.4	0.0159	3.6	0.836
11EGC30-14.1	0.120	947	186	0.20	12.97	102.1 ± 1.9	102.0 ± 1.9	62.63	1.9	0.0490	1.6	62.63	1.9	0.0490	1.6	0.1079	2.5	0.0160	1.9	0.774
11EGC30-20.1	0.123	1211	330	0.28	16.59	101.8 ± 1.5	102.0 ± 1.5	62.63	1.4	0.0490	1.4	62.79	1.4	0.0470	2.2	0.1031	2.6	0.0159	1.4	0.545
11EGC30-19.1	0.167	1829	262	0.15	25.11	102.2 ± 1.5	102.2 ± 1.5	62.49	1.5	0.0494	1.1	62.55	1.5	0.0486	1.4	0.1071	2.1	0.0160	1.5	0.727

11EGC30-22.1	0.104	2660	982	0.38	36.51	102.3 ± 1.5	102.2 ± 1.5	62.52	1.5	0.0489	1.0	62.54	1.5	0.0486	1.0	0.1072	1.8	0.0160	1.5	0.814
11EGC30-2.1	0.030	2769	1059	0.40	38.06	102.2 ± 2.2	102.3 ± 2.2	62.48	2.2	0.0483	0.9	62.55	2.2	0.0475	1.2	0.1046	2.5	0.0160	2.2	0.883
11EGC30-23.1	0.070	1846	401	0.22	25.41	102.4 ± 2.1	102.5 ± 2.1	62.38	2.1	0.0486	1.1	62.42	2.1	0.0481	1.3	0.1061	2.5	0.0160	2.1	0.840
11EGC30-15.1	0.143	2520	950	0.39	34.77	102.7 ± 1.8	102.7 ± 1.8	62.17	1.8	0.0492	1.0	62.26	1.8	0.0481	1.3	0.1064	2.2	0.0161	1.8	0.806
11EGC30-3.1	0.071	2303	1137	0.51	31.85	102.9 ± 2.3	102.9 ± 2.3	62.08	2.2	0.0487	1.0	62.14	2.2	0.0479	1.2	0.1063	2.5	0.0161	2.2	0.874
11EGC30-17.1	--	1669	262	0.16	23.10	102.8 ± 2.3	103.0 ± 2.3	62.13	2.3	0.0473	1.2	62.23	2.3	0.0461	1.6	0.1021	2.8	0.0161	2.3	0.812
11EGC30-16.1	--	2341	1195	0.53	32.44	103.1 ± 1.4	103.2 ± 1.4	62.01	1.4	0.0477	1.0	62.04	1.4	0.0473	1.2	0.1052	1.8	0.0161	1.4	0.770
11EGC30-5.1	0.159	854	415	0.50	11.88	103.3 ± 2.4	103.6 ± 2.4	61.65	2.3	0.0494	3.3	61.89	2.3	0.0464	4.3	0.1033	4.8	0.0162	2.3	0.477
11EGC30-10.1	0.034	2838	795	0.29	39.49	103.5 ± 1.8	103.6 ± 1.8	61.72	1.8	0.0484	0.9	61.79	1.8	0.0475	1.2	0.1060	2.1	0.0162	1.8	0.840
11EGC30-24.1	0.042	1498	223	0.15	20.87	103.7 ± 1.4	103.7 ± 1.4	61.62	1.4	0.0484	1.2	61.64	1.4	0.0482	1.3	0.1078	1.9	0.0162	1.4	0.713
11EGC30-13.1	0.008	683	132	0.20	9.53	103.7 ± 1.0	103.8 ± 1.0	61.58	1.0	0.0482	1.8	61.65	1.0	0.0472	2.3	0.1056	2.5	0.0162	1.0	0.384
11EGC30-18.1	--	3367	1198	0.37	47.75	105.5 ± 2.4	105.6 ± 2.4	60.60	2.3	0.0477	1.8	60.60	2.3	0.0477	1.8	0.1085	2.9	0.0165	2.3	0.786
11EGC30-8.1	--	220	138	0.65	3.13	106.5 ± 1.3	106.0 ± 1.2	60.35	1.2	0.0477	3.1	60.04	1.2	0.0517	5.3	0.1188	5.5	0.0167	1.2	0.219
~~11EGC30-6.1~~	~~0.286~~	~~15426~~	~~1206~~	~~0.08~~	~~253.9~~	~~122.6 ± 13.3~~	~~122.3 ± 13.3~~	~~52.04~~	~~10.9~~	~~0.0507~~	~~7.5~~	~~52.00~~	~~10.9~~	~~0.0501~~	~~7.6~~	~~0.1326~~	~~13.3~~	~~0.0192~~	~~10.9~~	~~0.821~~
~~11EGC30-9.1~~	~~0.142~~	~~1103~~	~~144~~	~~0.13~~	~~28.29~~	~~189.8 ± 5.0~~	~~189.6 ± 5.0~~	~~33.46~~	~~2.7~~	~~0.0510~~	~~1.0~~	~~33.46~~	~~2.7~~	~~0.0509~~	~~1.1~~	~~0.2096~~	~~2.9~~	~~0.0299~~	~~2.7~~	~~0.929~~
~~11EGC30-25.1~~	~~0.394~~	~~1242~~	~~480~~	~~0.40~~	~~36.27~~	~~215.7 ± 9.6~~	~~215.5 ± 9.6~~	~~29.30~~	~~4.5~~	~~0.0536~~	~~0.9~~	~~29.39~~	~~4.5~~	~~0.0513~~	~~1.4~~	~~0.2405~~	~~4.7~~	~~0.0340~~	~~4.5~~	~~0.958~~
~~11EGC30-7.1~~	~~0.511~~	~~234~~	~~139~~	~~0.61~~	~~17.43~~	~~538.6 ± 60.7~~	~~536.5 ± 61.5~~	~~11.46~~	~~11.7~~	~~0.0622~~	~~1.4~~	~~11.48~~	~~11.7~~	~~0.0613~~	~~1.6~~	~~0.7369~~	~~11.9~~	~~0.0871~~	~~11.7~~	~~0.991~~
~~11EGC30-4.1~~	~~0.449~~	~~235~~	~~106~~	~~0.47~~	~~18.28~~	~~560.6 ± 13.3~~	~~558.4 ± 13.5~~	~~11.00~~	~~2.5~~	~~0.0622~~	~~1.2~~	~~11.01~~	~~2.5~~	~~0.0619~~	~~1.2~~	~~0.7760~~	~~2.0~~	~~0.0909~~	~~2.5~~	~~0.893~~

Sample EG15, quartz monzodiorite; 177.22468 E, 69.185379 N

Spot	% $^{206}Pb_c$	ppm U	ppm Th	$^{232}Th/^{238}U$	ppm $^{206}Pb^*$	(1) $^{206}Pb/^{238}U$ Age	(2) $^{206}Pb/^{238}U$ Age	Total $^{238}U/^{206}Pb$	± %	Total $^{207}Pb/^{206}Pb$	± %	(1) $^{238}U/^{206}Pb^*$	± %	(1) $^{207}Pb^*/^{206}Pb^*$	± %	(1) $^{207}Pb^*/^{235}U$	± %	(1) $^{206}Pb^*/^{238}U$	± %	err corr
11EGC15-16	--	1986	187	0.10	26.71	100.1 ± 1.0	100.1 ± 1.0	63.93	1.0	0.0473	1.2	63.92	1.0	0.0474	1.3	0.1023	1.6	0.0156	1.0	0.638
11EGC15-9	--	1222	539	0.46	16.99	103.2 ± 1.2	103.5 ± 1.2	61.86	1.2	0.0470	1.6	61.99	1.2	0.0454	2.0	0.1010	2.4	0.0161	1.2	0.500
11EGC15-12	0.100	881	488	0.57	12.31	104.1 ± 1.9	104.0 ± 1.9	61.45	1.8	0.0489	1.8	61.43	1.8	0.0492	1.9	0.1105	2.6	0.0163	1.8	0.680
11EGC15-11	--	613	489	0.82	8.57	103.9 ± 1.3	104.1 ± 1.3	61.51	1.2	0.0468	2.1	61.55	1.3	0.0463	2.4	0.1037	2.7	0.0162	1.3	0.465
11EGC15-5	0.098	1049	256	0.25	14.68	104.4 ± 0.6	104.1 ± 0.6	61.34	0.6	0.0489	1.7	61.27	0.6	0.0498	1.9	0.1120	2.0	0.0163	0.6	0.281
11EGC15-15	0.056	1029	214	0.21	14.42	104.4 ± 1.9	104.3 ± 1.9	61.27	1.8	0.0486	1.6	61.27	1.8	0.0486	1.6	0.1093	2.4	0.0163	1.8	0.749
11EGC15-14	0.148	770	242	0.32	10.79	104.1 ± 1.7	104.4 ± 1.7	61.17	1.6	0.0493	1.8	61.44	1.6	0.0458	3.1	0.1029	3.5	0.0163	1.6	0.462
11EGC15-8	0.028	1291	365	0.29	18.14	104.7 ± 2.1	104.6 ± 2.1	61.10	2.0	0.0483	1.5	61.06	2.0	0.0488	1.6	0.1102	2.6	0.0164	2.0	0.786
11EGC15-13	0.080	929	339	0.38	13.11	105.0 ± 1.3	105.0 ± 1.3	60.83	1.2	0.0488	1.7	60.90	1.2	0.0479	2.0	0.1084	2.4	0.0164	1.2	0.524
11EGC15-1	--	1284	468	0.38	18.18	105.1 ± 1.6	105.4 ± 1.6	60.76	1.5	0.0469	3.0	60.84	1.5	0.0459	3.3	0.1039	3.6	0.0164	1.5	0.426
11EGC15-3	--	652	218	0.35	9.30	105.8 ± 0.6	106.2 ± 0.6	60.28	0.6	0.0473	2.0	60.41	0.6	0.0457	2.8	0.1043	2.8	0.0166	0.6	0.208
11EGC15-6	--	2243	667	0.31	32.08	106.2 ± 1.7	106.4 ± 1.7	60.11	1.7	0.0476	1.1	60.21	1.7	0.0463	1.4	0.1060	2.2	0.0166	1.7	0.763
11EGC15-2	--	1273	334	0.27	18.30	106.9 ± 1.3	107.0 ± 1.3	59.79	1.2	0.0477	1.5	59.82	1.2	0.0473	1.6	0.1090	2.0	0.0167	1.2	0.597
11EGC15-7	--	1157	314	0.28	16.66	106.8 ± 1.8	107.2 ± 1.8	59.75	1.7	0.0470	2.9	59.84	1.7	0.0458	3.2	0.1055	3.6	0.0167	1.7	0.469
11EGC15-10	0.034	1574	477	0.31	22.76	107.5 ± 1.5	107.6 ± 1.5	59.40	1.4	0.0485	1.4	59.44	1.4	0.0479	1.5	0.1111	2.1	0.0168	1.4	0.683
11EGC15-4	0.043	1924	801	0.43	28.09	108.7 ± 1.9	108.6 ± 1.9	58.82	1.7	0.0486	1.2	58.81	1.7	0.0487	1.2	0.1142	2.1	0.0170	1.7	0.817

Sample EG11A, deformed monzodiorite; 177.214669 E, 69.184725 N

Spot	% $^{206}Pb_c$	ppm U	ppm Th	$^{232}Th/^{238}U$	ppm $^{206}Pb^*$	(1) $^{206}Pb/^{238}U$ Age	(2) $^{206}Pb/^{238}U$ Age	Total $^{238}U/^{206}Pb$	± %	Total $^{207}Pb/^{206}Pb$	± %	(1) $^{238}U/^{206}Pb^*$	± %	(1) $^{207}Pb^*/^{206}Pb^*$	± %	(1) $^{207}Pb^*/^{235}U$	± %	(1) $^{206}Pb^*/^{238}U$	± %	err corr
EGC11A-8.1	0.14	579	289	0.52	7.89	100.1 ± 1.0	101.4 ± 1.0	63.00	1.0	0.0491	3.5	63.21	1.0	0.0466	4.6	0.1017	4.7	0.0158	1.0	0.215
EGC11A-5.1	0.02	997	402	0.42	13.76	103.2 ± 2.3	102.7 ± 2.3	62.24	2.3	0.0483	2.5	62.48	2.3	0.0453	3.4	0.1001	4.1	0.0160	2.3	0.555
EGC11A-6.1	0.69	543	334	0.64	7.65	104.1 ± 1.5	104.8 ± 1.5	60.57	1.4	0.0536	3.4	60.90	1.4	0.0492	5.0	0.1115	5.2	0.0164	1.4	0.276
EGC11A-3.1	0.19	1335	517	0.40	18.85	105.1 ± 2.1	105.2 ± 2.1	60.69	2.0	0.0497	2.2	60.73	2.0	0.0491	2.4	0.1115	3.1	0.0165	2.0	0.644
EGC11A-10.1	--	707	200	0.29	9.99	105.8 ± 0.8	105.2 ± 0.8	60.90	0.8	0.0466	3.1	61.16	0.8	0.0431	4.6	0.0971	4.6	0.0163	0.8	0.168
EGC11A-1.1	--	1220	350	0.30	17.26	106.2 ± 1.7	105.3 ± 1.7	60.73	1.6	0.0480	2.4	60.82	1.6	0.0469	2.7	0.1063	3.1	0.0164	1.6	0.505
EGC11A-4.1	0.26	959	348	0.38	13.58	106.9 ± 1.7	105.4 ± 1.7	60.50	1.6	0.0502	2.7	60.56	1.6	0.0494	2.9	0.1125	3.4	0.0165	1.6	0.484
EGC11A-9.1	--	912	328	0.37	13.06	106.8 ± 0.6	106.6 ± 0.6	60.03	0.6	0.0477	2.7	60.11	0.6	0.0466	3.1	0.1069	3.2	0.0166	0.6	0.185
EGC11A-7.1	0.48	194	85	0.45	2.78	107.5 ± 0.8	106.6 ± 0.9	59.70	0.8	0.0520	5.7	59.70	0.8	0.0520	5.7	0.1201	5.8	0.0168	0.8	0.131
EGC11A-2.1	0.55	760	248	0.34	11.09	108.7 ± 1.3	108.6 ± 1.3	58.57	1.2	0.0525	3.1	58.67	1.2	0.0511	3.5	0.1202	3.7	0.0170	1.2	0.314

Sample EG31, potassic gabbro dike; 177.152401 E, 69.224268 N

Spot	% $^{206}Pb_c$	ppm U	ppm Th	$^{232}Th/^{238}U$	ppm $^{206}Pb^*$	(1) $^{206}Pb/^{238}U$ Age	(2) $^{206}Pb/^{238}U$ Age	Total $^{238}U/^{206}Pb$	± %	Total $^{207}Pb/^{206}Pb$	± %	(1) $^{238}U/^{206}Pb^*$	± %	(1) $^{207}Pb^*/^{206}Pb^*$	± %	(1) $^{207}Pb^*/^{235}U$	± %	(1) $^{206}Pb^*/^{238}U$	± %	err corr
EGC31-10.1	--	180	8	0.05	2.38	96.7 ± 1.7	98.4 ± 1.6	65.11	1.6	0.0467	6.6	66.17	1.8	0.0339	18.2	0.0707	18.3	0.0151	1.8	0.097
EGC31-11.1	0.17	461	54	0.12	6.10	98.3 ± 0.7	98.4 ± 0.7	64.89	0.7	0.0493	4.0	65.11	0.7	0.0467	5.3	0.0989	5.4	0.0154	0.7	0.127
EGC31-8.1	0.18	566	63	0.12	7.49	98.6 ± 0.7	98.5 ± 0.8	64.82	0.7	0.0494	3.5	64.88	0.8	0.0487	3.8	0.1036	3.9	0.0154	0.8	0.192
EGC31-6.1	0.08	224	49	0.23	2.98	98.3 ± 0.8	98.8 ± 0.8	64.67	0.7	0.0487	5.7	65.09	0.8	0.0436	9.3	0.0923	9.3	0.0154	0.8	0.087
EGC31-5.1	0.29	425	92	0.22	5.69	99.8 ± 1.3	99.8 ± 1.3	63.91	1.3	0.0503	4.0	64.12	1.3	0.0477	5.3	0.1026	5.5	0.0156	1.3	0.243
EGC31-1.1	0.41	299	68	0.23	4.00	100.0 ± 1.3	99.9 ± 1.3	63.76	1.3	0.0513	4.8	63.97	1.3	0.0487	6.3	0.1050	6.5	0.0156	1.3	0.202
EGC31-3.1	--	544	170	0.32	7.34	99.8 ± 1.3	100.4 ± 1.3	63.85	1.3	0.0465	3.6	64.12	1.3	0.0432	5.3	0.0928	5.4	0.0156	1.3	0.241
EGC31-7.1	0.37	313	61	0.20	4.22	100.9 ± 1.5	100.4 ± 1.5	63.49	1.4	0.0510	4.7	63.39	1.5	0.0522	5.2	0.1135	5.4	0.0158	1.5	0.271
EGC31-13.1	--	250	30	0.12	3.39	100.0 ± 0.8	101.0 ± 0.8	63.47	0.7	0.0463	5.4	63.94	0.8	0.0403	9.7	0.0870	9.8	0.0156	0.8	0.082
EGC31-2.1	0.01	602	53	0.09	8.28	102.3 ± 0.6	102.4 ± 0.6	62.42	0.6	0.0482	3.4	62.52	0.6	0.0470	3.9	0.1036	4.0	0.0160	0.6	0.152
EGC31-9.1	--	952	371	0.40	13.10	102.2 ± 1.3	102.5 ± 1.3	62.47	1.2	0.0474	2.8	62.59	1.3	0.0459	3.4	0.1010	3.6	0.0160	1.3	0.349
EGC31-4.1	0.05	298	135	0.47	4.10	102.5 ± 1.1	102.5 ± 1.1	62.38	1.0	0.0485	5.1	62.38	1.0	0.0485	5.1	0.1071	5.2	0.0160	1.0	0.202
EGC31-12.1	--	220	168	0.79	3.12	103.6 ± 2.0	105.3 ± 2.0	61.13	1.9	0.0429	5.9	61.73	2.0	0.0350	12.5	0.0782	12.6	0.0162	2.0	0.156

Sample EG35A, migmatite (unpolished rims); 177.040939 E, 69.26353 N

Spot	% $^{206}Pb_c$	ppm U	ppm Th	$^{232}Th/^{238}U$	ppm $^{206}Pb^*$	(1) $^{206}Pb/^{238}U$ Age	(2) $^{206}Pb/^{238}U$ Age	Total $^{238}U/^{206}Pb$	± %	Total $^{207}Pb/^{206}Pb$	± %	(1) $^{238}U/^{206}Pb^*$	± %	(1) $^{207}Pb^*/^{206}Pb^*$	± %	(1) $^{207}Pb^*/^{235}U$	± %	(1) $^{206}Pb^*/^{238}U$	± %	err corr
EGC35A-1.1	--	2162	40	0.019	30.05	103.5 ± 2.6	103.7 ± 2.6	61.65	2.5	0.0481	3.0	61.79	2.5	0.0462	3.5	0.1031	4.3	0.01618	2.5	0.582
EGC35A-2.1	0.32	2119	9	0.004	29.11	102.3 ± 1.9	102.4 ± 1.9	62.27	1.8	0.0507	1.5	62.54	1.8	0.0472	2.7	0.1040	3.3	0.01599	1.8	0.562
~~EGC35A-3.1~~	~~0.14~~	~~1482~~	~~9~~	~~0.007~~	~~24.10~~	~~120.9 ± 21.0~~	~~120.8 ± 21.1~~	~~52.79~~	~~17.6~~	~~0.0496~~	~~1.8~~	~~52.81~~	~~17.6~~	~~0.0492~~	~~2.0~~	~~0.1286~~	~~17.7~~	~~0.01893~~	~~17.6~~	~~0.994~~
~~EGC35A-4.1~~	~~0.81~~	~~1120~~	~~14~~	~~0.013~~	~~24.74~~	~~163.7 ± 34.9~~	~~163.6 ± 35.0~~	~~38.59~~	~~21.6~~	~~0.0560~~	~~3.5~~	~~38.88~~	~~21.6~~	~~0.0500~~	~~4.8~~	~~0.1772~~	~~22.1~~	~~0.02572~~	~~21.6~~	~~0.976~~
EGC35A-5.1	0.38	2951	178	0.062	40.88	103.1 ± 2.3	103.1 ± 2.3	61.81	2.2	0.0512	1.2	62.01	2.2	0.0486	2.0	0.1081	3.0	0.01613	2.2	0.751
EGC35A-6.1	0.38	1634	10	0.006	23.09	105.2 ± 1.2	105.2 ± 1.2	60.52	1.2	0.0513	1.7	60.80	1.2	0.0475	3.1	0.1077	3.3	0.01645	1.2	0.354
~~EGC35A-7.1~~	~~0.37~~	~~826~~	~~37~~	~~0.047~~	~~30.83~~	~~274.4 ± 32.3~~	~~274.3 ± 32.6~~	~~22.92~~	~~12.0~~	~~0.0548~~	~~2.7~~	~~23.00~~	~~12.0~~	~~0.0518~~	~~3.3~~	~~0.3105~~	~~12.5~~	~~0.04348~~	~~12.0~~	~~0.964~~
EGC35A-8.1	0.16	2503	10	0.004	33.56	99.82 ± 1.7	100.2 ± 1.7	63.72	1.7	0.0494	1.4	64.08	1.7	0.0448	2.9	0.0963	3.4	0.01561	1.7	0.514
EGC35A-9.1	0.85	1422	16	0.012	19.39	101.5 ± 2.0	101.5 ± 2.0	62.47	2.0	0.0550	2.0	63.02	2.0	0.0479	4.6	0.1047	5.0	0.01587	2.0	0.407
~~EGC35A-10.1~~	~~0.76~~	~~1774~~	~~7~~	~~0.004~~	~~33.52~~	~~140.2 ± 11.6~~	~~140.0 ± 11.6~~	~~45.20~~	~~8.4~~	~~0.0550~~	~~1.3~~	~~45.48~~	~~8.4~~	~~0.0500~~	~~2.7~~	~~0.1516~~	~~8.8~~	~~0.02199~~	~~8.4~~	~~0.951~~
EGC35A-12.1	0.39	1270	6	0.005	17.14	100.5 ± 10.3	101.0 ± 10.4	63.07	10.3	0.0513	4.8	63.67	10.3	0.0435	7.1	0.0942	12.5	0.01571	10.3	0.825
EGC35A-11.1	0.93	1284	10	0.008	18.72	108.5 ± 12.6	108.4 ± 12.7	58.42	11.8	0.0558	4.0	58.92	11.8	0.0489	5.8	0.1144	13.1	0.01697	11.8	0.896

91500 zircon (1065 Ma), secondary standard used on unpolished rim mount

Spot	% $^{206}Pb_c$	ppm U	ppm Th	$^{232}Th/^{238}U$	ppm $^{206}Pb^*$	(1) $^{206}Pb/^{238}U$ Age	(2) $^{206}Pb/^{238}U$ Age	Total $^{238}U/^{206}Pb$	± %	Total $^{207}Pb/^{206}Pb$	± %	(1) $^{238}U/^{206}Pb^*$	± %	(1) $^{207}Pb^*/^{206}Pb^*$	± %	(1) $^{207}Pb^*/^{235}U$	± %	(1) $^{206}Pb^*/^{238}U$	± %	err corr
91500-1.1	0.88	62	21	0.34	9.6	1068 ±35	1074 ±37	5.500	3.5	0.0780	2.1	5.548	3.6	0.0710	4.2	1.764	5.5	0.18023	3.6	0.645
91500-3.1	0.76	64	22	0.36	10.2	1100 ±16	1104 ±17	5.334	1.6	0.0795	2.1	5.375	1.6	0.0735	3.8	1.886	4.1	0.18604	1.6	0.382
91500-2.1	--	49	14	0.29	7.4	1048 ±16	1041 ±17	5.666	1.7	0.0796	2.4	5.666	1.7	0.0796	2.4	1.937	2.9	0.17650	1.7	0.581
91500-3.2	0.74	61	20	0.34	9.3	1059 ±16	1063 ±17	5.558	1.6	0.0778	4.1	5.599	1.7	0.0720	5.6	1.772	5.8	0.17859	1.7	0.283

Errors are 1σ; Pb_c and Pb^* indicate the common and radiogenic portions, respectively.

Errors in standard calibration (1σ) VE samples: 0.36%; EG35A: 0.34%; EG11A & EG31: 0.25%; EG15: 0.32%; EG30: 0.43%; EG6, EG8 & EG33A: 0.46%.

(1) Common Pb corrected using measured ^{204}Pb.

(2) Common Pb corrected by assuming $^{206}Pb/^{238}U$-$^{207}Pb/^{235}U$ age-concordance

SUPPLEMENTARY DATA TABLE S3 40Ar/39 DATA

VELITKENAY, CHUKOTKA 40AR/39AR DATA

Sample 11EGC35A (BIOTITE, 0.45 mg) Diode - PID Regulated Step-Heating

Step	Current (Amps)	Temp (°C) (needs to be updated relative to calibration file)		40Ar/39Ar[1]	38Ar/39Ar[1]	37Ar/39Ar[1]	36Ar/39Ar[1]	39Ar (mol)[2]	39Ar (%)	40Ar*[3] (%)	40Ar*/39Ar[3]	± 1 s.d.	Model Age (Ma)	± 1 s.d.
1	5.1		180	206.4583	0.1515093	36.57461	0.6438849	2.08E-17	9.93E-02	6.615035	19.3843	5.0732	63.87517	16.42481
2	5.4		180	34.33078	3.86E-02	2.295397	1.89E-02	6.91E-16	3.39419	78.40428	28.94652	0.1332	94.57071	0.4239925
3	5.7		180	29.69452	3.62E-02	0.9519403	1.53E-03	6.26E-15	33.2753	97.8151	29.32875	######	95.78691	9.85E-02
4	6		180	29.53292	3.58E-02	0.9735769	4.01E-04	2.41E-15	44.796	97.44051	29.50191	######	96.3376	0.1273463
5	6.2		180	29.75673	3.56E-02	1.497467	4.45E-04	1.05E-15	49.8129	94.79221	29.76266	######	97.16656	0.2549119
6	6.4		180	29.86531	0.0359676	0.7924162	5.61E-04	5.90E-16	52.6268	91.3227	29.77009	0.1556	97.19016	0.4946792
7	6.6		180	29.99422	0.0364034	0.4424132	1.03E-03	9.69E-16	57.2522	92.36233	29.72752	######	97.05486	0.2606069
8	6.8		180	29.61105	3.61E-02	1.449849	6.78E-04	1.39E-15	63.8728	95.71319	29.54344	######	96.46967	0.1973817
9	7		180	29.43724	3.59E-02	1.774002	4.38E-04	1.33E-15	70.2076	95.80012	29.47099	######	96.2393	0.2270846
10	7.5		180	29.44246	3.63E-02	1.233339	4.69E-04	2.77E-15	83.4238	97.71709	29.41584	######	96.0639	0.1338562
11	9		180	29.50348	3.60E-02	0.9532809	5.93E-04	3.42E-15	99.7339	97.97384	29.41401	######	96.05808	0.113227
12	12		180	37.71257	0.0409107	4.320558	2.26E-02	5.58E-17	99.99	46.14743	31.45188	1.3814	102.5275	4.377592
J-Factor:	**1.859E-03 ± 1.851E-05**													

Sample 11EGC35A (BIOTITE, 0.22 mg) Diode - PID Regulated Step-Heating

Step	Current (Amps)	Temp (°C) (needs to be updated relative to calibration file)		40Ar/39Ar[1]	38Ar/39Ar[1]	37Ar/39Ar[1]	36Ar/39Ar[1]	39Ar (mol)[2]	39Ar (%)	40Ar*[3] (%)	40Ar*/39Ar[3]	± 1 s.d.	Model Age (Ma)	± 1 s.d.
1	5.1		180	403.1222	0.3691897	0	1.266379	7.18E-18	5.55E-02	4.545662	28.90263	16.375	94.48348	52.15121
2	5.4		180	34.97696	3.94E-02	1.752288	1.77E-02	3.91E-16	3.07833	75.76471	29.8945	0.199	97.63972	0.6326661
3	5.7		180	29.51414	3.65E-02	0.9013004	1.17E-03	4.37E-15	36.8369	97.74032	29.25023	######	95.59021	0.1066463
4	6		180	29.4463	3.62E-02	0.6921351	3.90E-04	1.75E-15	50.3976	96.60799	29.3921	######	96.04173	0.2044784
5	6.2		180	29.64501	3.64E-02	1.211987	8.71E-04	5.92E-16	54.9695	90.62063	29.49789	0.1287	96.37835	0.4093995
6	6.4		180	29.75136	3.60E-02	3.970507	8.60E-04	4.52E-16	58.4637	88.8748	29.86909	0.1651	97.55896	0.524847
7	6.6		180	29.75269	3.67E-02	1.245236	9.13E-04	7.06E-16	63.9171	92.12855	29.59634	0.1089	96.69154	0.3463693
8	6.8		180	29.40347	0.0360655	1.651301	-2.79E-05	8.70E-16	70.6386	93.91741	29.56349	######	96.58704	0.2885165
9	7		180	29.59977	3.68E-02	1.05307	4.15E-04	7.36E-16	76.324	92.79906	29.57241	0.1121	96.61542	0.3565495
10	7.5		180	29.53968	3.62E-02	1.447781	5.00E-04	1.31E-15	86.4619	95.65257	29.52438	######	96.46263	0.2196152
11	9		180	29.66187	3.64E-02	0.8961278	1.27E-03	1.72E-15	99.7565	95.72671	29.36791	######	95.96478	0.185525
12	12		180	53.2333	5.28E-02	15.54231	8.63E-02	3.15E-17	99.99	27.36964	29.19633	2.2367	95.41865	7.120092
J-Factor:	**1.860E-03 ± 1.852E-05**													

Sample 11EGC33A (HORNBLENDE, 1.82 mg) Diode - PID Regulated Step-Heating

Step	Current (Amps)	Temp (°C) (needs to be updated relative to calibration file)		40Ar/39Ar[1]	38Ar/39Ar[1]	37Ar/39Ar[1]	36Ar/39Ar[1]	39Ar (mol)[2]	39Ar (%)	40Ar*[3] (%)	40Ar*/39Ar[3]	± 1 s.d.	Model Age (Ma)	± 1 s.d.
1	6.25		180	616.2743	0.3979817	17.50792	1.78737	1.21E-16	1.09583	14.12321	90.5047	4.2665	280.8751	12.26151
2	6.75		180	45.47647	6.35E-02	2.931939	4.58E-02	1.90E-16	2.82394	58.06853	32.21175	0.5245	105.0501	1.661779
3	7.25		180	41.54048	0.1268014	5.283504	3.74E-02	7.71E-16	9.83305	70.32541	31.00244	0.1396	101.2149	0.4432054
4	7.75		180	34.24572	0.1360454	3.850033	0.0152553	3.32E-15	40.0124	86.1992	30.09892	######	98.34406	0.1512566
5	8		180	30.96336	0.1364624	3.72469	6.03E-03	5.50E-15	90.0343	94.08076	29.52884	######	96.53034	0.1133568
6	8.33		180	32.75861	0.1366135	4.490249	1.14E-02	4.40E-16	94.0345	81.16577	29.80128	0.1982	97.39733	0.6305434
7	8.67		180	33.10752	0.1285124	2.861599	0.0121536	4.72E-16	98.3221	81.64417	29.7828	0.1784	97.33854	0.5677686
8	9		180	35.07269	0.137249	2.367376	0.0184656	1.18E-16	99.3982	60.81133	29.83605	0.5908	97.50794	1.879712
9	10		180	38.25749	0.1373539	6.998189	3.19E-02	6.62E-17	99.99	47.02377	29.4755	1.3479	96.36053	4.290954
J-Factor:	**1.861E-03 ± 1.854E-05**													

Sample 11EGC33A (BIOTITE, 1.70 mg) Diode - PID Regulated Step-Heating

Step	Current (Amps)	Temp (°C) (needs to be updated relative to calibration file)	40Ar/39Ar[1]	38Ar/39Ar[1]	37Ar/39Ar[1]	36Ar/39Ar[1]	39Ar (mol)[2]	39Ar (%)	40Ar*[3] (%)	40Ar*/39Ar[3]	± 1 s.d.	Model Age (Ma)	± 1 s.d.
1	5.1	180	352.587	0.2460104	14.71129	1.163407	4.55E-17	5.00E-02	2.533931	9.985452	3.9557	33.24265	13.04839
2	5.4	180	55.04102	5.57E-02	1.35041	0.1431742	5.01E-16	0.60075	21.90785	12.84054	0.263	42.63601	0.862944
3	5.7	180	34.37439	3.32E-02	0.8786912	1.94E-02	5.03E-15	6.13592	82.63839	28.72668	######	94.02732	0.1404502
4	6	180	29.61548	2.95E-02	0.8856241	1.93E-03	1.63E-14	24.076	97.86814	29.12492	######	95.297	0.1704404
5	6.2	180	29.39958	0.0293669	0.9306037	1.13E-03	1.07E-14	35.8896	98.49651	29.14849	0.0381	95.37209	0.1213036
6	6.4	180	29.83848	2.97E-02	1.133169	2.18E-03	7.81E-15	44.481	97.30575	29.29617	######	95.8427	0.1057642
7	6.6	180	29.90421	2.98E-02	1.018195	1.90E-03	6.85E-15	52.0152	97.46214	29.43502	######	96.28505	0.1032134
8	6.8	180	29.66395	2.94E-02	0.9063669	1.10E-03	4.94E-15	57.4475	97.92867	29.41966	######	96.23611	9.90E-02
9	7	180	29.44899	2.97E-02	0.9404671	7.12E-04	4.33E-15	62.2097	97.99118	29.32308	######	95.92844	0.1093963
10	7.5	180	29.22673	0.0293576	0.8885961	7.52E-04	9.70E-15	72.8791	98.80614	29.08399	######	95.16653	0.1131312
11	9	180	29.24445	2.92E-02	1.079536	1.10E-03	2.16E-14	96.6852	98.74265	29.01708	######	94.95326	0.219569
12	12	180	29.56433	0.0289816	1.233924	1.73E-03	3.01E-15	99.99	96.63778	29.1644	######	95.42282	0.115812

J-Factor: 1.862E-03 ± 1.855E-05

Sample 11EGC24 (BIOTITE, 0.21 mg) Diode - PID Regulated Step-Heating

Step	Current (Amps)	Temp (°C) (needs to be updated relative to calibration file)	40Ar/39Ar[1]	38Ar/39Ar[1]	37Ar/39Ar[1]	36Ar/39Ar[1]	39Ar (mol)[2]	39Ar (%)	40Ar*[3] (%)	40Ar*/39Ar[3]	± 1 s.d.	Model Age (Ma)	± 1 s.d.
1	5.5	180	35.32959	2.66E-02	1.942518	3.00E-02	1.40E-15	14.9965	72.45642	26.63511	######	87.44134	0.2850527
2	6	180	30.56427	2.37E-02	0.8231252	2.75E-03	3.14E-15	48.6739	95.7299	29.82603	######	97.63824	0.125067
3	6.2	180	32.54359	2.51E-02	1.098738	1.82E-03	7.73E-16	56.9741	92.22083	32.10864	0.1137	104.8973	0.3608181
4	6.5	180	34.62335	0.0268228	0.4684483	1.39E-03	1.10E-15	68.8238	94.38306	34.2548	######	111.6959	0.2493858
5	6.8	180	33.12464	2.59E-02	1.665769	1.88E-03	9.58E-16	79.1092	93.52264	32.72599	######	106.8556	0.278519
6	7	180	26.1035	2.14E-02	7.651896	-1.88E-02	2.28E-16	81.5616	71.08428	32.38329	0.3132	105.7688	0.9933951
7	7.5	180	31.69729	2.61E-02	1.08092	2.42E-03	7.64E-16	89.7641	91.50931	31.08006	0.1179	101.6299	0.3750034
8	8	180	32.20864	2.57E-02	0.7039652	3.23E-03	6.07E-16	96.2838	89.38058	31.31588	0.1276	102.3795	0.4054773
9	10	180	32.88607	2.62E-02	0.6067799	7.54E-03	3.46E-16	99.99	81.69598	30.71171	0.2372	100.4583	0.7546158

J-Factor: 1.865E-03 ± 1.857E-05

Sample 11EGC15 (BIOTITE, 2.51 mg) Diode - PID Regulated Step-Heating

Step	Current (Amps)	Temp (°C) (needs to be updated relative to calibration file)	40Ar/39Ar[1]	38Ar/39Ar[1]	37Ar/39Ar[1]	36Ar/39Ar[1]	39Ar (mol)[2]	39Ar (%)	40Ar*[3] (%)	40Ar*/39Ar[3]	± 1 s.d.	Model Age (Ma)	± 1 s.d.
1	5.75	180	33.01038	2.93E-02	1.2674	2.08E-02	6.89E-15	8.78204	81.02781	26.99033	######	88.62846	0.1279811
2	6.25	180	29.60276	2.57E-02	1.092116	6.30E-04	1.93E-14	33.3403	99.30376	29.51532	######	96.70136	0.1982937
3	6.75	180	30.02016	2.62E-02	1.074681	6.14E-04	1.39E-14	51.0742	99.21297	29.9361	######	98.04317	0.1506026
4	7.25	180	29.67019	2.60E-02	1.023711	4.16E-04	1.15E-14	65.753	99.30022	29.63962	######	97.09782	0.1284675
5	7.75	180	29.48109	0.0271818	1.160281	4.83E-04	9.24E-15	77.5299	99.14653	29.44349	######	96.47221	0.1111742
6	8	180	29.51903	2.58E-02	1.212914	6.71E-04	4.25E-15	82.9522	97.96188	29.43104	######	96.43248	0.1105705
7	8.33	180	29.5373	2.57E-02	1.281902	5.97E-04	3.99E-15	88.0345	98.22257	29.4775	######	96.58071	0.1150371
8	8.67	180	29.50422	2.56E-02	1.216863	5.46E-04	3.98E-15	93.1056	98.22302	29.45353	0.0314	96.50423	0.1000235
9	9	180	29.58158	2.61E-02	1.211544	6.28E-04	3.38E-15	97.4083	97.89108	29.50605	######	96.67177	0.1125848
10	10	180	29.60971	2.68E-02	1.838071	6.37E-04	2.03E-15	99.99	95.84128	29.59084	######	96.94225	0.1692967

J-Factor: 1.866E-03 ± 1.858E-05

Sample 11EGC11B (HORNBLENDE, 4.56 mg) Diode - PID Regulated Step-Heating

Step	Current (Amps)	Temp (°C) (needs to be updated relative to calibration file)	40Ar/39Ar[1]	38Ar/39Ar[1]	37Ar/39Ar[1]	36Ar/39Ar[1]	39Ar (mol)[2]	39Ar (%)	40Ar*[3] (%)	40Ar*/39Ar[3]	± 1 s.d.	Model Age (Ma)	± 1 s.d.
1	5.5	180	567.5404	0.415745	17.56849	1.825148	1.13E-16	0.75077	5.056975	29.86997	3.4473	97.88651	10.99624
2	6	180	126.721	0.0928103	5.443439	0.3215653	1.87E-16	1.99683	23.62694	32.21894	0.7996	105.3637	2.539861
3	6.5	180	58.63767	5.77E-02	9.957389	6.45E-02	1.10E-16	2.72739	55.07745	40.60357	0.8332	131.8034	2.60823
4	7	180	53.06035	6.84E-02	4.967041	5.67E-02	3.33E-16	4.95003	63.53658	36.79112	0.2892	119.8294	0.9113307

5	7.25	180	49.42006	6.03E-02	3.218773	2.68E-02	2.73E-16	6.77223	75.86082	41.8186	0.2904	135.6029	0.9070945
6	7.5	180	38.83187	5.34E-02	5.454519	1.71E-02	9.70E-16	13.2366	84.44184	34.31169	0.1109	111.9992	0.3509389
7	7.75	180	32.85768	4.78E-02	4.61156	9.03E-03	7.82E-15	65.3998	92.21323	30.62573	######	100.2956	0.119879
8	8	180	31.91492	4.60E-02	4.550989	5.35E-03	4.89E-15	97.9814	94.98457	30.76372	######	100.7351	0.11635
9	10	180	41.7432	5.26E-02	3.275117	0.0371761	3.03E-16	99.99	58.36845	31.06644	0.3064	101.6989	0.9751564

J-Factor: **1.867E-03 ± 1.859E-05**

Flux Monitor: **Taylor Creek Sanidine (28.34 Ma)**
40Ar/39ArK: **4.400E-03 ± 6.000E-04**
38Ar/39ArK: **1.282E-02 ± 2.000E-05**
36Ar/37ArCa: **2.500E-04 ± 2.500E-05**
39Ar/37ArCa: **7.000E-04 ± 7.000E-05**

Analytical errors (±1 s.d.) only. Systematic errors such as those associated with radioactive decay or irradiation correction factors are not propagated
[1]Raw data corrected for ion counter deadtime; instrumental mass fractionation; proceedural line blank; & radioactive decay of 37Ar 39Ar & 36Cl
[2]Total 39Ar normalized to 100% delivery to the Mass Spectrometer
[3]Corrected for nuclear interferences & trapped Ar (40Ar/36Ar = 295.5)

TABLE S3 CONTINUED

WRANGEL ISLAND 40Ar/39Ar DATA

SAMPLE ELM06 WR 11B (K-FELDSPAR; 1.77MG) Diode-Current Regulated Step-Heating

Step	Current (Amps	Temp (°C)	Time (s)	40Ar/39Ar[1]	38Ar/39Ar[1]	37Ar/39Ar[1]	36Ar/39Ar[1]	39Ar (mol)[2]	39Ar (%)	40Ar*[3] (%)	40Ar*/39Ar[3]	± 1 s.d.	Model Age (Ma	± 1 s.d.
1	5.00	409	180	343.161	9.9549E-02	-	4.432E-01	4.020E-17	0.02	53.44	212.18	3.29	559.48	7.45
2	5.00	409	180	468.914	1.3110E-01	-	6.642E-01	9.984E-18	0.03	39.76	272.65	11.22	691.60	23.65
3	5.20	436	180	2368.060	6.6505E-02	-	2.670E-01	3.337E-16	0.2	96.38	2289.17	6.19	2875.41	3.89
4	5.20	438	180	246.185	2.5358E-02	-	6.060E-02	8.988E-17	0.3	83.85	228.28	1.61	595.60	3.57
5	5.40	504	180	294.923	1.7457E-02	-	2.267E-02	5.791E-15	3.5	97.57	288.22	0.27	724.12	0.55
6	5.40	509	180	47.461	1.3093E-02	-	2.460E-03	1.700E-15	4.5	95.28	46.73	0.06	138.98	0.18
7	5.60	588	180	67.776	1.3600E-02	-	4.161E-03	8.429E-15	9.2	97.83	66.55	0.07	194.81	0.20
8	5.60	589	180	36.619	1.2883E-02	-	8.156E-04	1.720E-15	10.1	96.21	36.38	0.06	109.09	0.16
9	5.80	646	180	46.394	1.3186E-02	-	1.777E-03	4.155E-15	12.5	97.88	45.87	0.04	136.50	0.13
10	5.80	643	180	35.142	1.3001E-02	-	5.857E-04	1.540E-15	13.3	96.05	34.97	0.06	104.99	0.19
11	6.00	692	180	48.014	1.3115E-02	-	1.386E-03	3.517E-15	15.3	98.06	47.60	0.05	141.47	0.13
12	6.00	691	180	34.805	1.2787E-02	-	4.771E-04	1.614E-15	16.2	96.39	34.66	0.05	104.10	0.15
13	6.20	728	180	42.176	1.3156E-02	-	1.203E-03	2.761E-15	17.8	97.59	41.82	0.05	124.86	0.13
14	6.40	762	180	44.762	1.3038E-02	-	1.511E-03	3.747E-15	19.8	97.91	44.32	0.04	132.04	0.13
15	6.60	789	180	39.842	1.3145E-02	-	9.883E-04	3.768E-15	22.0	98.04	39.55	0.04	118.30	0.11
16	6.80	814	180	37.249	1.2802E-02	-	8.333E-04	3.727E-15	24.0	98.18	37.00	0.04	110.91	0.11
17	7.00	835	180	36.378	1.2881E-02	-	6.265E-04	3.559E-15	26.0	98.15	36.19	0.05	108.55	0.13
18	7.20	853	180	36.466	1.3005E-02	-	7.082E-04	3.226E-15	27.8	97.92	36.26	0.04	108.74	0.11
19	7.40	865	180	37.137	1.2910E-02	-	8.786E-04	2.628E-15	29.3	97.49	36.88	0.04	110.54	0.12
20	7.60	886	180	38.782	1.3227E-02	-	1.052E-03	2.741E-15	30.9	97.61	38.47	0.05	115.17	0.13
21	7.80	903	180	41.121	1.3026E-02	-	1.303E-03	2.411E-15	32.2	97.57	40.74	0.05	121.73	0.13
22	8.00	920	180	44.927	1.3200E-02	-	1.886E-03	2.215E-15	33.4	97.14	44.37	0.06	132.20	0.18
23	8.20	938	180	48.431	1.3320E-02	-	2.280E-03	2.171E-15	34.7	97.02	47.76	0.06	141.91	0.17
24	8.40	955	180	51.892	1.3359E-02	-	2.683E-03	2.255E-15	35.9	97.04	51.10	0.06	151.43	0.17
25	8.60	974	180	53.775	1.3382E-02	-	3.003E-03	2.338E-15	37.2	97.04	52.89	0.06	156.51	0.16
26	8.80	991	180	55.372	1.3646E-02	-	3.516E-03	2.271E-15	38.5	96.94	54.33	0.07	160.60	0.18
27	9.00	1007	180	57.326	1.3575E-02	-	3.946E-03	2.353E-15	39.8	96.77	56.16	0.07	165.76	0.19
28	9.25	1028	180	59.838	1.3719E-02	-	4.543E-03	2.886E-15	41.4	96.84	58.50	0.06	172.33	0.17
29	9.50	1047	180	63.789	1.4274E-02	-	7.355E-03	3.600E-15	43.5	95.87	61.62	0.07	181.08	0.18
30	9.75	1063	180	67.318	1.3845E-02	-	4.899E-03	5.019E-15	46.3	97.34	65.87	0.06	192.94	0.16
31	10.00	1077	180	70.755	1.3935E-02	-	4.724E-03	7.646E-15	50.5	97.71	69.36	0.07	202.60	0.20
32	10.25	1094	180	72.604	1.3774E-02	-	4.493E-03	1.222E-14	57.4	97.96	71.28	0.10	207.89	0.27
33	10.50	1110	180	73.308	1.3623E-02	-	3.991E-03	1.871E-14	67.9	98.26	72.13	0.15	210.24	0.40
34	10.75	1123	180	71.491	1.3566E-02	-	3.708E-03	2.246E-14	80.4	98.36	70.40	0.17	205.46	0.47
35	11.00	1138	180	69.820	1.3456E-02	-	3.318E-03	2.084E-14	92.1	98.47	68.84	0.15	201.16	0.43
36	11.25	1153	180	68.790	1.3232E-02	-	2.890E-03	1.026E-14	97.9	98.53	67.94	0.08	198.67	0.23
37	11.50	1172	180	66.734	1.3138E-02	-	2.412E-03	2.683E-15	99.4	98.06	66.02	0.08	193.35	0.22
38	11.75	1192	180	69.179	1.2549E-02	-	1.609E-03	6.641E-16	99.7	95.61	68.70	0.16	200.79	0.45

39	12.00	1218	180	68.090	1.2536E-02	-	-2.867E-04	2.955E-16	99.9	93.02	68.17	0.25	199.33	0.68
40	13.00	1275	180	58.600	1.2502E-02	-	4.581E-04	1.356E-16	100.0	84.17	58.46	0.44	172.25	1.23
41	14.00	1329	180	72.493	1.5911E-02	-	2.354E-02	2.452E-17	100.0	52.67	65.54	2.18	192.01	6.07
42	15.00	1364	180	63.890	1.2957E-02	-	-2.821E-02	1.010E-17	100.0	32.05	72.23	5.93	210.50	16.30

[1]Raw data corrected for ion counter deadtime; instrumental mass fractionation; proceedural line blank; & radioactive decay of 37Ar 39Ar & 36Cl
[2]Total 39Ar normalized to 100% delivery to the Mass Spectrometer
[3]Corrected for nuclear interferences & trapped Ar (40Ar/36Ar = 295.5)

Flux Monitor: Taylor Creek Sanidine (28.34 Ma)
J-Factor: 1.714E-03 ± 1.706E-05
40Ar/39ArK: 1.000E-04 ± 7.013E-04
38Ar/39ArK: 1.267E-02 ± 1.464E-05
36Ar/37ArCa: 2.892E-04 ± 8.283E-06
39Ar/37ArCa: 6.699E-04 ± 3.489E-06

SAMPLE ELM06 WR-11B (MUSCOVITE; 1.23 mg) Diode-Current Regulated Step-Heating

Step	Current (Amps	Temp (°C)	Time (s)	40Ar/39Ar[1]	38Ar/39Ar[1]	37Ar/39Ar[1]	36Ar/39Ar[1]	39Ar (mol)[2]	39Ar (%)	40Ar*[3] (%)	40Ar*/39Ar[3]	± 1 s.d.	Model Age (Ma)
1	5.1	425	180	193.37	6.538E-02	-	2.934E-01	5.391E-17	0.08	45.21	106.66	2.02	302.83
2	5.4	523	180	197.95	1.797E-02	-	2.302E-02	3.493E-16	0.57	93.55	191.15	0.56	511.17
3	5.7	642	180	203.32	1.377E-02	-	4.370E-03	2.609E-15	4.26	98.94	202.03	0.18	536.33
4	5.9	710	180	217.94	1.447E-02	-	8.857E-03	4.248E-15	10.28	98.54	215.32	0.18	566.59
5	6.1	758	180	239.93	1.326E-02	-	2.705E-03	1.172E-14	26.86	99.57	239.13	0.32	619.58
6	6.3	805	180	239.12	1.296E-02	-	8.229E-04	1.301E-14	45.28	99.81	238.87	0.34	619.01
7	6.6	1000	180	228.56	1.306E-02	-	1.307E-03	6.576E-15	54.59	99.65	228.17	0.20	595.38
8	6.9	1113	180	234.00	1.304E-02	-	1.100E-03	1.146E-14	70.81	99.73	233.67	0.30	607.57
9	7.5	1221	180	237.75	1.288E-02	-	9.059E-04	1.052E-14	85.70	99.77	237.48	0.29	615.96
10	8.5	1232	180	243.27	1.322E-02	-	1.869E-03	4.386E-15	91.91	99.50	242.72	0.20	627.43
11	9.5	1226	180	248.66	1.349E-02	-	3.558E-03	2.973E-15	96.12	99.18	247.60	0.22	638.06
12	12	1356	180	260.09	1.457E-02	-	9.238E-03	2.743E-15	99.99	98.55	257.37	0.26	659.12

[1]Raw data corrected for ion counter deadtime; instrumental mass fractionation; proceedural line blank; & radioactive decay of 37Ar 39Ar & 36Cl
[2]Total 39Ar normalized to 100% delivery to the Mass Spectrometer
[3]Corrected for nuclear interferences & trapped Ar (40Ar/36Ar = 295.5)

Flux Monitor: Taylor Creek Sanidine (28.34 Ma)
J-Factor: 1.714E-03 ± 1.706E-05
40Ar/39ArK: 1.000E-04 ± 7.013E-04
38Ar/39ArK: 1.267E-02 ± 1.464E-05
36Ar/37ArCa: 2.892E-04 ± 8.283E-06
39Ar/37ArCa: 6.699E-04 ± 3.489E-06

Analytical errors (±1 s.d.) only. Systematic errors such as those associated with radioactive decay or irradiation correction factors are not propagated

SAMPLE CGS C145701 (MUSCOVITE; 2.18 mg) Diode-Current Regulated Step-Heating

Step	Current (Amps	Temp (°C)	Time (s)	40Ar/39Ar[1]	38Ar/39Ar[1]	37Ar/39Ar[1]	36Ar/39Ar[1]	39Ar (mol)[2]	39Ar (%)	40Ar*[3] (%)	40Ar*/39Ar[3]	± 1 s.d.	Model Age (Ma)
1	5.1	0	180	253.21	1.398E-01	-	6.812E-01	2.229E-17	0.03	14.02	51.92	5.30	153.76
2	5.4	0	180	158.17	2.805E-02	-	7.409E-02	3.009E-16	0.37	81.63	136.28	0.54	378.65
3	5.7	0	180	177.85	1.646E-02	-	1.965E-02	1.545E-15	2.13	95.85	172.05	0.23	466.13
4	5.9	0	180	202.51	1.486E-02	-	1.054E-02	2.486E-15	4.97	97.96	199.39	0.20	530.26
5	6.1	0	180	223.21	1.406E-02	-	6.144E-03	4.650E-15	10.28	98.94	221.40	0.20	580.27
6	6.3	0	180	247.29	1.335E-02	-	3.319E-03	2.065E-14	33.85	99.54	246.31	0.54	635.25
7	6.6	0	180	229.12	1.298E-02	-	1.161E-03	1.292E-14	48.60	99.75	228.78	0.32	596.73
8	6.9	0	180	214.28	1.326E-02	-	1.916E-03	7.340E-15	56.98	99.56	213.72	0.20	562.97
9	7.5	0	180	231.36	1.316E-02	-	1.963E-03	1.043E-14	68.88	99.62	230.78	0.28	601.18
10	8.5	0	180	235.90	1.307E-02	-	1.011E-03	9.295E-15	79.49	99.67	235.60	0.25	611.83
11	9.5	0	180	247.11	1.302E-02	-	5.463E-04	6.657E-15	87.09	99.77	246.95	0.23	636.65
12	12	0	180	249.76	1.286E-02	-	5.750E-04	1.131E-14	99.99	99.84	249.59	0.32	642.37

[1]Raw data corrected for ion counter deadtime; instrumental mass fractionation; proceedural line blank; & radioactive decay of 37Ar 39Ar & 36Cl

[2]Total 39Ar normalized to 100% delivery to the Mass Spectrometer

[3]Corrected for nuclear interferences & trapped Ar (40Ar/36Ar = 295.5)

Flux Monitor: Taylor Creek Sanidine (28.34 Ma)
J-Factor: 1.714E-03 ± 1.706E-05
40Ar/39ArK: 1.000E-04 ± 7.013E-04
38Ar/39ArK: 1.267E-02 ± 1.464E-05
36Ar/37ArCa: 2.892E-04 ± 8.283E-06
39Ar/37ArCa: 6.699E-04 ± 3.489E-06

Analytical errors (±1 s.d.) only. Systematic errors such as those associated with radioactive decay or irradiation correction factors are not propagated

SAMPLE ELM06 WR-28B (MUSCOVITE; 2.53 mg) Diode-Current Regulated Step-Heating

Sample 28BMUS (MUS; 2.59 mg) Diode - Current Regulated Step-Heating

Step	Current (Amps	Temp (°C)	Time (s)	40Ar/39Ar[1]	38Ar/39Ar[1]	37Ar/39Ar[1]	36Ar/39Ar[1]	39Ar (mol)[2]	39Ar (%)	40Ar*[3] (%)	40Ar*/39Ar[3]	± 1 s.d.	Model Age (Ma)
1	5.2	0	180	755.68	4.307E-01	-	2.245E+00	2.168E-17	0.02	10.66	92.40	13.39	265.17
2	5.5	0	180	275.85	7.777E-02	-	3.452E-01	1.464E-16	0.17	59.51	173.86	1.33	470.44
3	5.7	0	180	186.20	2.864E-02	-	8.270E-02	1.722E-15	1.96	86.24	161.76	0.23	441.38
4	5.9	0	180	189.29	2.425E-02	-	6.036E-02	2.684E-15	4.75	90.14	171.46	0.19	464.71
5	6.1	0	180	194.70	2.280E-02	-	5.330E-02	3.722E-15	8.61	91.60	178.95	0.19	482.51
6	6.3	0	180	206.93	1.864E-02	-	3.115E-02	9.677E-15	18.66	95.43	197.73	0.24	526.41
7	6.6	0	180	199.76	1.434E-02	-	8.243E-03	3.044E-14	50.27	98.73	197.33	0.64	525.48
8	6.9	0	180	185.31	1.384E-02	-	6.442E-03	2.233E-15	52.59	98.16	183.41	0.21	493.03
9	7.5	0	180	191.02	1.415E-02	-	6.748E-03	5.236E-15	58.02	98.62	189.03	0.15	506.21
10	8.5	0	180	196.03	1.373E-02	-	4.969E-03	1.926E-14	78.03	99.17	194.56	0.40	519.09
11	9.5	0	180	190.91	1.327E-02	-	2.576E-03	1.397E-14	92.53	99.52	190.15	0.29	508.82
12	12	0	180	191.05	1.318E-02	-	1.696E-03	4.422E-15	97.12	99.49	190.55	0.18	509.75
13	12	0	180	195.14	1.307E-02	-	1.500E-03	2.771E-15	99.99	99.37	194.69	0.19	519.39

[1]Raw data corrected for ion counter deadtime; instrumental mass fractionation; proceedural line blank; & radioactive decay of 37Ar 39Ar & 36Cl

²Total 39Ar normalized to 100% delivery to the Mass Spectrometer
³Corrected for nuclear interferences & trapped Ar (40Ar/36Ar = 295.5)

Flux Monitor:	Taylor Creek Sanidine (28.34 Ma)
J-Factor:	1.714E-03 ± 1.706E-05
40Ar/39ArK:	1.000E-04 ± 7.013E-04
38Ar/39ArK:	1.267E-02 ± 1.464E-05
36Ar/37ArCa:	2.892E-04 ± 8.283E-06
39Ar/37ArCa:	6.699E-04 ± 3.489E-06

Analytical errors (±1 s.d.) only. Systematic errors such as those associated with radioactive decay or irradiation correction factors are not propagated

TABLE S4: Apatite fission track age data, track length data, and methods

Sample number	Irradiation number	No xls	Spontaneous		Induced		$P(\chi^2)$ (%)	Dosimeter		Central age (Ma)	1s on age (Ma)	No len	Mean track length (μm)	1s on mean length (μm)	Std dev (μm)	Dpar range (µm)	Sample quality
			Rho-S	NS	Rho-I	NI		Rho-D	ND								
WR-1A	SU075-01	20	1.0545	1389	2.6701	3517	15.5	1.1628	3536	88.0	3.5	100	13.88	0.14	1.37	1.34-1.89	Good
WR-2	SU075-04	20	1.1573	1161	2.7891	2798	23.3	1.1886	3536	95.2	4.0	95	13.79	0.10	1.02	1.38-1.99*	Fair to good
WR-7B	SU075-05	25	0.7570	624	1.7493	1442	24.0	1.1886	3536	98.4	5.2	13	13.13	0.24	0.86	1.41-2.16	Poor; age rough
WR-8	SU075-06	9	0.9268	100	2.4466	264	18.0	1.2058	3536	87.7	10.6	--	--	--	--	--	V. poor; age rough
WR-9	SU075-07	27	1.2884	774	2.9529	1774	1.8	1.2058	3536	101.0	6.1	69	14.15	0.11	0.93	1.39-2.13*	Poor
WR-10B	SU075-08	11	1.6305	317	3.6570	711	21.3	1.2230	3536	105.0	7.8	--	--	--	--	--	V. poor; age rough
WR-11B	SU075-10	6	4.0953	1262	10.8517	3344	23.3	1.2402	3536	89.7	3.4	100	13.86	0.12	1.15	1.44-1.89	Poor

Note: Full sample numbers are of the form ELM06-WR-1A. Abbreviations are: No xls, number of individual crystals (grains) dated; Rho-S, spontaneous track density (x 10^6 tracks per square centimeter); NS, number of spontaneous tracks counted; Rho-I, induced track density in muscovite external detector (x 10^6 tracks per square centimeter); NI, number of induced tracks counted; $P(\chi^2)$, χ^2 probability (Galbraith, 1981; Green, 1981); Rho-D, induced track density in external detector adjacent to dosimetry glass (x 10^6 tracks per square centimeter); ND, number of tracks counted in determining Rho-D; No len, number of track length measured; Std dev, standard deviation of the track length distribution. Dpar range, range of Dpar values measured in crystals that were dated plus in crystals in which track lengths were measured, * indicates a 1 or 3 Dpar measurements were discarded (see below); Age is the sample central fission track age (Galbraith and Laslett, 1993), calculated using zeta calibration method (Hurford and Green, 1983). Analyst: T.A. Dumitru.

The following is a summary of key laboratory procedures. Apatites were etched for 20 s in 5N nitric acid at 20°C. Grains were dated by external detector method with muscovite detectors. Samples were irradiated in well thermalized positions of Oregon State University reactor. CN5 dosimetry glasses with muscovite external detectors were used as neutron flux monitors. External detectors were etched in 48% HF. Tracks counted with Zeiss Axioskop microscope with 100x air objective, 1.25x tube factor, 10x eyepieces, transmitted light with supplementary reflected light as needed; external detector prints were located with Kinetek automated scanning stage (Dumitru, 1993). Only grains with c axes subparallel to slide plane were dated. Ages calculated using zeta calibration factor of 385.9. Confined tracks lengths were measured only in apatite grains with c axes subparallel to slide plane; only horizontal tracks measured (within ±≈5-10°), following protocols of Laslett et al. (1982). Lengths were measured with computer digitizing tablet and drawing tube, calibrated against stage micrometer (Dumitru, 1993). Angles of confined tracks to their host grains' c-axes and the Dpar track entrance diameter where also measured, following protocols of Ketcham et al. (2007), except that confined tracks hosted by both surface tracks and by cleavage surfaces were measured. Age calculations were done with spreadsheet by J.P. Colgan.

The following is a summary of thermal history modeling methods. Modeling done with the Hefty 1.7.4 program of Ketcham et al. (2007). Modeling parameters: (1) used raw track length data (actual lengths, Dpar, and angle to c-axis of each track) and actual track counts (NS, NI, and Dpar of each grain); (2) used annealing model of Ketcham et al. (2007) with Dpar kinetic variable; (3) due to narrow range of Dpar values, retained all track lengths and age grains for modeling as a single population, except discarded one length from WR-2 due to a higher dpar of 2.34 microns and one age and two lengths from WR-9 due to higher Dpar of 2.34, 2.49, and 2.64 microns; (4) modeled using midpoint value of Dpar range; (5) for length reduction in age standard, used default value of 0.893; (6) for initial track length, used default relations Lom=(0.258)(Dpar)+15.391 μm and Loc=(0.287)(Dpar)+15.582 μm; (7) projected track lengths to c-axis parallel equivalents using 20-sec – 20°C – 5.0M-HNO3 etchant option; (8) calculated 10000 model paths with Monte Carlo scheme and random subsegment spacing; (9) output plots show good model fit paths (red; merit value >0.5; accessed using Kuiper's statistic) and acceptable model fit paths (green; >0.05). (10) histograms of c-projected length in Figure 13 replotted manually due to minor bug in Hefty 1.7.4 histograms. No adjustments made for likely minor interlaboratory differences in length reduction in age standard or initial track length relationships between Ketcham et al (2007) and our laboratory.

References cited:

Dumitru, T.A., 1993, A new computer-automated microscope stage system for fission track analysis: Nuclear Tracks and Radiation Measurements, v. 21, p. 575-580.

Galbraith, R.F., 1981, On statistical models for fission track counts: Mathematical Geology, v. 13, p. 471-478.

Galbraith, R.F., and Laslett, G.M., 1993, Statistical models for mixed fission track ages: Nuclear Tracks and Radiation Measurements, v. 21, p. 459-470.

Green, P.F., 1981, A new look at statistics in fission-track dating: Nuclear Tracks and Radiation Measurements, v. 5, p. 77-86.

Hurford, A.J., and Green, P.F., 1983, The zeta age calibration of fission-track dating: Chemical Geology, v. 41, p. 285-317.

Ketcham, R.A., Carter, A, Donelick, R.A., Barbarand, J., and Hurford, A.J., 2007, Improved modeling of fission-track annealing in apatite: American Mineralogist, v. 92, p. 799-810. doi: 10.2138/am.2007.2281

Laslett, G.M., Kendall, W.S., Gleadow, A.J.W., and Duddy, I.R., 1982, Bias in the measurement of fission track length distributions: Nuclear Tracks and Radiation Measurements, v. 6, p. 79-85.

Supplementary Data: Appendix SA

EBSD Analysis of Quartz Lattice Preferred Orientations of quartz

Analytical Methods: Electron Back Scatter Diffraction analyses of Lattice Preferred Orientations (LPO's) of quartz: Two thin sections were polished for 1 hour with 1 μm and 0.25 μm diamond polishing compound, for 12–14 h in colloidal silica, and then carbon coated. They were analyzed at U.C. Santa Barbara in a JEOL 6300 scanning electron microscope fitted with an HKL Nordlys EBSD camera. They were inclined 70° to the incident beam. Working conditions were: 20 kV acceleration voltage, at 4.5 nA beam current, <1 μm spot size, and 25 mm working distance. Diffraction patterns were collected and indexed using CHANNEL 5 HKL software. By carefully examining the effect of parameters such as Hough transform, number of reflectors, minimum and maximum number of bands detected, and the chosen match unit, we are confident that the CHANNEL software indexed the correct phase >95% of the time. Samples were analyzed in both coarse and fine mode. Coarse scans used a step size of 50 μm designed to gather the bulk LPO of the sample and covered an area of 1 cm^2, whereas fine scans used a step size of 4 μm to examine textural attributes of samples and individual grains. We used the noise reduction system within the HKL software, carefully comparing our maps to the band contrast and fore scatter images to fill grains without artificially growing them. Sample data and results are presented below in Appendix SA of Supplementary Data and are discussed in more general fashion in the text under "Results, Wrangel Island".

Results: Deformation observed in sample ELM06 WR41, the quartzo-feldspathic grit, is similar to that of other quartzo-feldspathic grits, but the asymmetry of the fabric is stronger (Fig. SA 1(a), (b)). At the thin-section scale, two foliations, S and S' are seen

and the older one, S, which is deflected by S', indicates a top-to-the-south sense of shear (Figs. SA 1(a) and (b)). Deformation is dominated by formation of a phyllitic cleavage that wraps around quartz and feldspar grains (Fig. SA 1(c)). Heterogeneous deformation is due to the greater ease with which the surrounding matrix material and finer grained sedimentary and volcanic rock fragments accommodate strain in comparison to the detrital quartz and feldspar grains (Fig. SA 1(b) and (c)). Feldspar behaves as rigid porphyroclasts while quartz porphyroclasts have undergone flattening by crystal plastic slip leading to undulatory extinction and subgrain formation (Figs. SA 1(c) and (d)). At a smaller scale, the process of grain size reduction occurs primarily by bulging recrystallization (BLG) along subgrain boundaries and along the edges/boundaries of detrital quartz grains (Fig. SA 1(d)) (e.g. Stipp *et al*. 2002; Passhier & Trouw 2005), which is typical of high strain rocks deformed at low greenschist facies conditions (<~400°, Stipp *et al*. 2002). Three small regions of the thin-section were chosen for investigating quartz LPO's in more detail (Figs. SA 2,3). The area shown in Figure SA 2 consists of large, internally deformed detrital quartz grains mantled by fine-grained, dynamically recrystallized quartz in a matrix consisting of mica and quartz-rich bands (Figs. SA 2(a,b,c)). Fig. SA 2(b) and (c) highlight, respectively, the crystallographic orientations of large (> 1000 μm) and small (50-1000 μm) quartz grains based on band contrast + Euler angle maps constructed at ~1 μm resolution using ~ 0.5 million indexed points. Grains smaller than 50 μm were eliminated because they can be artifacts of the measurement process. Undulatory extinction and subgrain development can be seen in the large flattened and stretched detrital quartz grains while the smaller quartz grains (mostly in the matrix) are equant. A band contrast + Euler angle map of one of the large

quartz grains (Fig. SA 2 (d)) illustrates lattice misorientation with respect to a central point in the grain with maximum misorientations of 20° at the tips compared to the central point (Fig. 9(d)). Subgrain boundaries defined by misorientations of <1° are shown by thin white lines in the quartz grain (Fig. SA 2(d)). The large grain shows smoothly varying progressive misorientations away from the grain core toward both grain tips suggesting deformation by dislocation glide. Grain boundaries defined by misorientations of >15° are shown by thick white lines and separate the porphyroclastic quartz grain from the surrounding small grains. These large misorientations suggest that the small grains are not related to the large grain (nor to each other) through the process of subgrain rotation (e.g. Stipp *et al*. 2002). The lattice preferred orientations measured in the large grains (Fig. SA 2(e)) are insufficient to determine their statistical orientation but are similar to those measured in the small grains (Figs. SA 2 (e, f)). The small grains show a very weak lattice preferred orientation of C axes most similar to a Type-II crossed girdle pattern typical of co-axial deformation at lower greenschist grade (Schmidt & Casey, 1986) with perhaps a weak asymmetry suggesting a component of non-coaxial top-to-the-south shear (e.g. Lister, 1977; Law *et al*. 2004; Passchier & Trouw, 2005). The very weak fabric in the small grains suggest non LPO-producing deformation processes were active during deformation such as dynamic recrystallization, grain-boundary sliding or solution-transfer creep in addition to dislocation glide/creep. The <a> directions are also very weak and lie mostly close to the Z-X plane except for one concentration near the Y strain axis.

Figure SA 3 shows the results of EBSD studies on two additional very small areas of sample ELM06 WR-41. These sites are within fine-grained, thin, quartz-rich bands or

seams chosen for analysis because they appeared to have preferred LPO's during initial microscope inspection. Area 1 (location shown in Fig. SA 1(a)) is characterized by a weak oblique grain shape fabric that suggests top-to-the-north asymmetry (Fig. SA 3(a,b)) and yields a weak C-axis distribution transitional between a Type-II crossed girdle to a single girdle, with asymmetry indicating top-to-the-north shear, and the development of a very weak asymmetric distribution of < a > compatible with this interpretation (Fig. SA 3(c)) (e.g. Passchier &Trouw, 2005). Area 6 (Fig. SA 1(a)) lies at the termination of a top-to-the-south shear zone (Figs. SA 3(d,e,f)). This area has a weak grain shape foliation that suggests top-to-the-south shear (Figs. SA 3 (f) and (e)) and yielded a C-axis distribution that is also transitional between a Type-II crossed girdle to a single girdle, with asymmetry indicating a top-to the-south sense of shear and appropriate asymmetry developed in < a > (Fig. SA 3(g)).

The results of the second sample, the deformed aplite dike of granitic composition, (ELM06 WR28B), are illustrated in Figure SA 4. This sample was collected from the same (and only) exposure in which we measured top-to-the-south sense of shear indicators in the field (shear bands, S-C relations and mica fish seen as small steps on foliation surfaces). In thin section, this rock consists of quartz, feldspar and minor mica. Feldspar is cracked, pulled apart, boudinaged and rotated in a brittle and rigid fashion. Quartz and finer-grained matrix, including mica, wrap around the feldspars. Rotation of feldspar, the shear bands formed on the sides of feldspar porphyroclasts, and feldspar boudins are asymmetric both to the north and south rather than consistently dipping one way, compatible with deformation by mostly pure shear. Three small regions or bands/seams of fine-grained matrix quartz surrounding feldspar porphyroclasts were

targeted for analysis (Fig. SA 4). Although we thought that quartz LPO's in these small regions might not be well-developed, compromised by the small size of the region indexed and the amount of impurities (micas and feldspar) and/or influenced by the strain fields/flow regimes developed around larger feldspar porphyroclasts, the areas yielded weak but variably asymmetric LPO's (Fig. SA 4). Area 4, characterized by a small quartz grain size showing a south-dipping grain shape foliation, suggesting top-to-the-north shear, yielded a weak C-axis girdle that is asymmetric to the north with a distinct maximum near the Y strain direction (Fig. SA 4 (a,b,c)). The < a > directions form a girdle in the X-Z plane or perpendicular to the C-axis maximum. The dark band in the middle of mapped Area 4 is albite, which appears to also have undergone dynamic recrystallization (Fig. SA 4(a)). Area 5, which lies in a zone of top-to-the south shear related to the flow-field developed around a feldspar porphyroclast (Fig. SA 4 (d)) has a weak quartz grain shape foliation that dips to the north, suggesting top-to-the-south shear. Area 5 yielded a weak C-axis girdle that is asymmetric to the south with a maximum close to the Y strain direction (Fig. SA 4(f)). A-axes form a girdle in the X-Z plane or perpendicular to the C axis maximum, with a slightly greater concentration perpendicular to the C-axis girdle. Area 6, which indexed quartz in a larger portion of the thin section, contains both top-to-the-north and top-to-the-south shear bands developed around feldspar porphyroclasts (Fig. SA 4(g,h)). The indexed area yields a weak C-axis girdle that is slightly asymmetric to the north with a maximum near the Y strain direction (Fig. SA 4(i)). The < a > directions form a girdle in the X-Z plane with a concentration that is symmetric about the X strain axis. Although the strain in this rock is at all scales compatible with bulk pure shear as interpreted to be the case in most of our samples

(flattening perpendicular to foliation plane and stretching in a N-S direction), the quartz LPO's indicate higher temperatures of deformation than elsewhere. It has been shown that with increasing temperature, the prism < a > slip system in quartz becomes more important (Wilson, 1975; Bouchez, 1977; Lister & Dornsiepen, 1982; Law, 1990) and Type II crossed girdles tend towards single girdles and develop a maximum around the Y-axis with the < a > directions becoming perpendicular to the C-axes girdles (Schmidt & Casey, 1986; Passchier & Trouw, 2005). These data thus indicate deformation at a higher temperature at this locality than at ELM06-WR-41, suggesting temperatures greater than ~400°C, compatible with the observed growth of biotite and albite in these rocks.

Temperature is an important but not unique factor in determining how quartz deforms. There is also a strong strain rate and differential stress dependence and the presence of water in the quartz lattice or along grain boundaries can significantly lower the temperatures of deformation (e.g. Passchier & Trouw, 2005). The observed deformation by dislocation glide in quartz on Wrangel Island is consistent with the low greenschist facies conditions observed, representing temperatures of ~ 300-400°C. In most of these rocks, the LPO's indicate quartz deformation mainly by basal slip in the <a> crystallographic directions, leading to undulose extinction and subgrain formation. Similarly, in most rocks, the common dynamic recrystallization mechanism is BLG (bulging) recrystallization which is also characteristic of this same temperature range (e.g. Stipp *et al*. 2002). The process of BLG recrystallization increases the free energy of grain boundaries and if left at the temperatures the deformation occurred, annealing or recovery takes place during static recrystallization. The preservation of quartz

deformation textures formed by BLG indicates that deformation continued into lower temperatures, pressures and strain rates where they became "frozen in" (e.g. Passchier &Trouw, 2005). Sample ELM06 WR28B, collected from the deepest structural levels exposed, where biotite is part of the metamorphic assemblage, shows evidence for increasing amounts of prism <a> slip and thus deformation at somewhat higher temperatures.

Despite the fairly large strains represented in the basement and sedimentary cover rocks of Wrangel Island, these rocks yield evidence for deformation dominated by pure shear flattening perpendicular to the foliation and N-S stretching within the foliation. The microstructures and quartz LPO's yield limited evidence for top-to-the-south shear, but some of the data show both senses of shear in individual thin-sections, compatible with our estimate that *bulk deformation was mostly by pure shear*. More importantly, the progression of textures upward in the structural section (to lesser penetrative strain) and the high degree of preservation of delicate quartz deformation textures (rather than their annealing), suggests that foliation development S_D on Wrangel Island was associated with deformation that led to rapid cooling and exhumation instead of thrust burial and thermal re-equilibration, which would have led to annealing of these textures. This conclusion is supported by the thermochronology data discussed in the text of this contribution.

References Cited:

Bouchez, J. L., 1977, Plastic deformation of quartzites at low temperatures in an area of natural strain gradient, Tectonophysics v. 39, p. 25-50.

Law, R.D., 1990, Crystallographic fabrics: a selective review of their applications to research in structural geology: In: Knipe, R. J. and Rutter, E. H., eds., Deformation mechanisms, rheology and tectonics, Geological Society of London Special Publication 54, p. 335-352.

Law, R. D., Searle, M. P., and Simpson, R. L., 2004, Strain, deformation temperatures and vorticity of flow at the top of the Greater Himalayan Slab, Everest Massif, Tibet, Journal of Geological Society of London v. 161, p. 305-320.

Lister, G.S., 1977, Discussion: crossed-girdle c-axis fabrics in quartzites plastically deformed by plane strain and progressive simple shear, Tectonophysics, v. 39, p. 51-54.

Lister, G.S. and Dornsiepen, U.F., 1982, Fabric transition in the Saxony granulite terrain, Journal of Structural Geology v. 41, p. 81-92.

Passchier. C.W. and Trouw, R.A. J., 2005, Microtectonics, Springer-Verlag, Berlin-Heidelberg, 366p.

Schmidt, S. M. and Casey, M., 1986, Complete fabric analysis of some commonly observed quartz [c]-axis patterns, in, Hobbs, B. E. and Heard, H. C., eds, Mineral and Rock Deformation: Laboratory Studies, Geophysical Monograph 36, p. 263-286.

Stipp, M., Stunitz, H., Heilbronner, R., Schmid, S. M., 2002, The eastern Tonale fault zone: a "natural laboratory for crystal plastic deformation of quartz over a temperature range from 250°C to 700°C. Journal of Structural Geology v. 24, p. 1861-1884.

Wilson, C. J. L., 1975, Preferred orientation in quartz ribbon mylonites, Geological Society of America Bulletin v. 86, p. 968-974.

Figure SA1 Miller et al. Wrangel Island

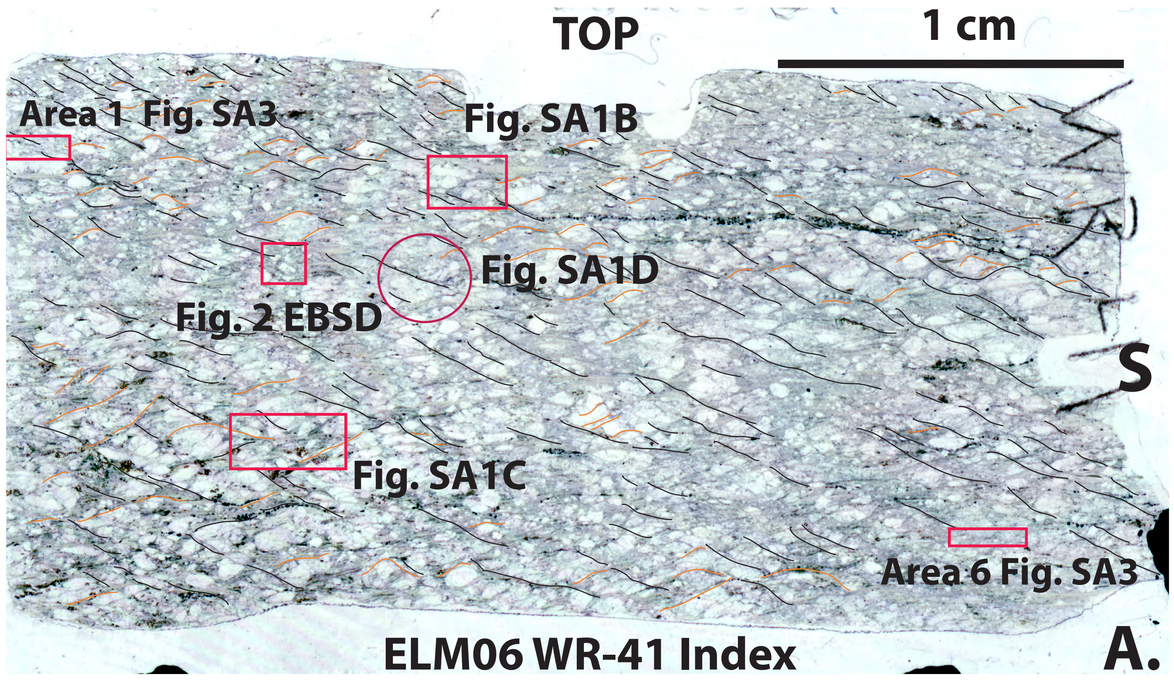

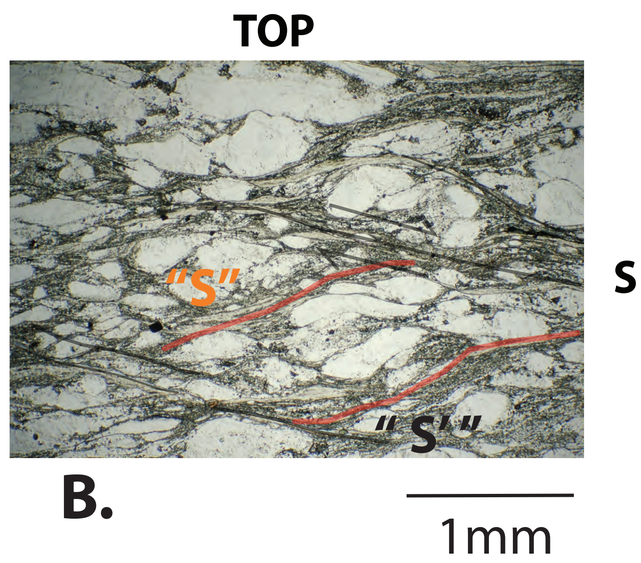

Top

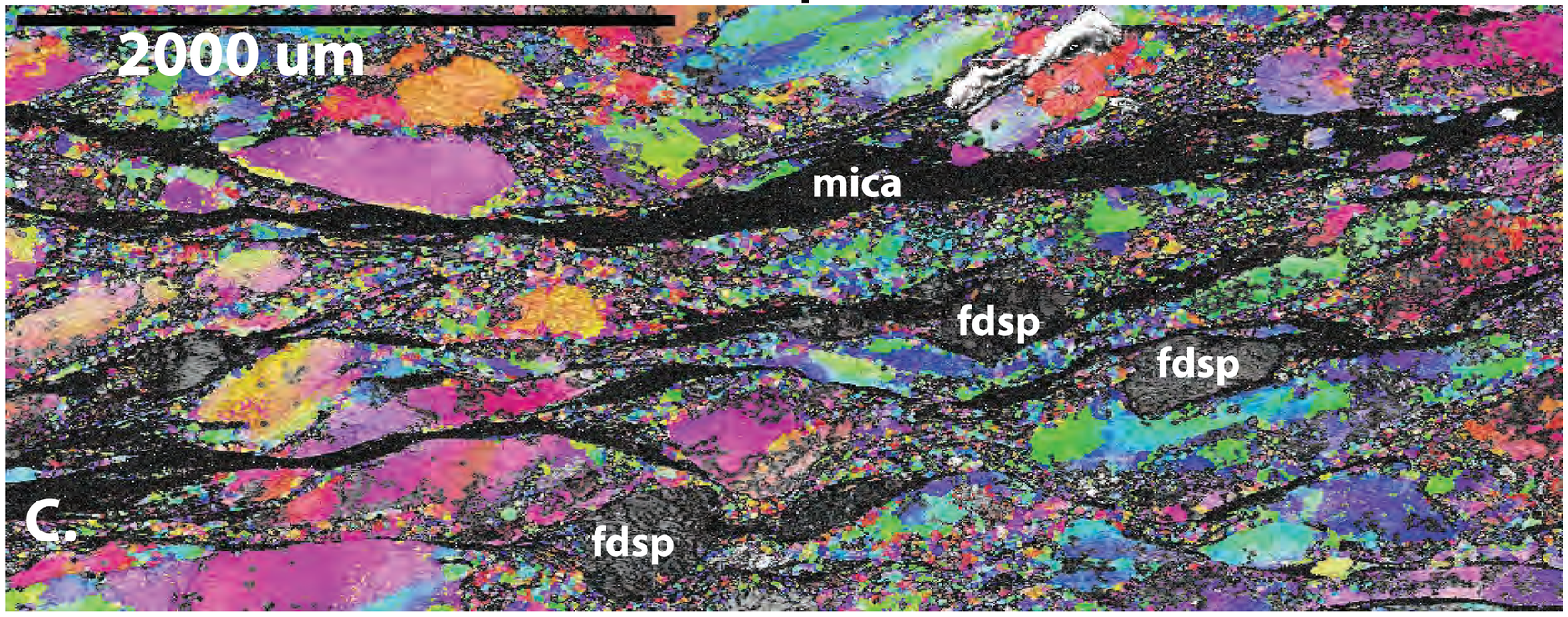

Top

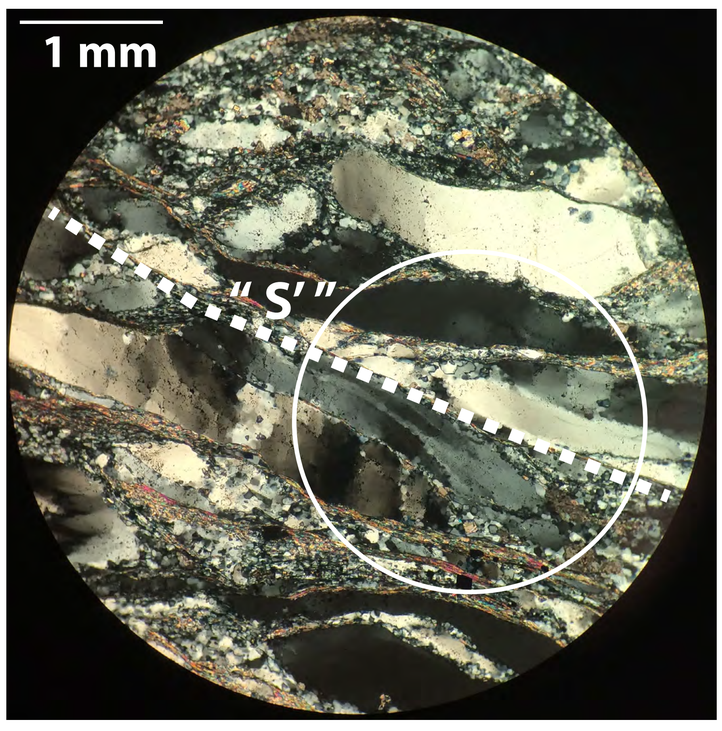

Top

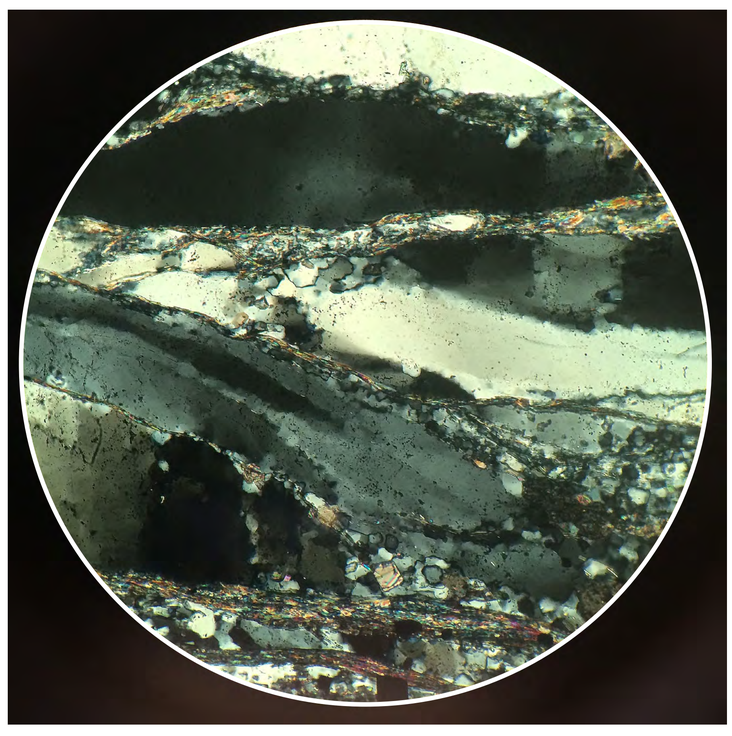

D.

Figure SA1. A. High resolution scan of oriented thin-section ELM06 WR-41, used as index map for photomicrographs and EBSD analysis (see Figure 2 for sample locality). S, South. South-dipping syn-metamorphic shear bands "S' ", mapped and highlighted in black, bend and offset schistosity, "S" suggesting top-to-the-south shear. B. Detail of A: photomicrograph of syn-metamorphic shear bands " S'" mapped in index map. C. EBSD band contrast + Euler angle map of a representative region of the thin section (for location see A) done at a coarse scan to determine how sample LPO's should be measured. The map C. shows that much of the deformation in the rock is taken up within the finer micaceous matrix and that larger detrital quartz and feldspar grains behave as semi-rigid to rigid porphyroclasts. The quartz grains have changed in shape by internal deformation by crystal plastic slip. Feldspar grains are rotated or brittlely deformed. The gray to black areas are feldspar and mica, which were excluded from imaging. D. Photomicrographs (inset shows higher power image) that provide detailed view of quartz deformation by dislocation glide and climb leading to undulatory extinction and subgrain formation in detrital quartz grains and by grain size reduction along subgrain boundaries and the edges of grains by mostly BLG (bulging recrystallization).

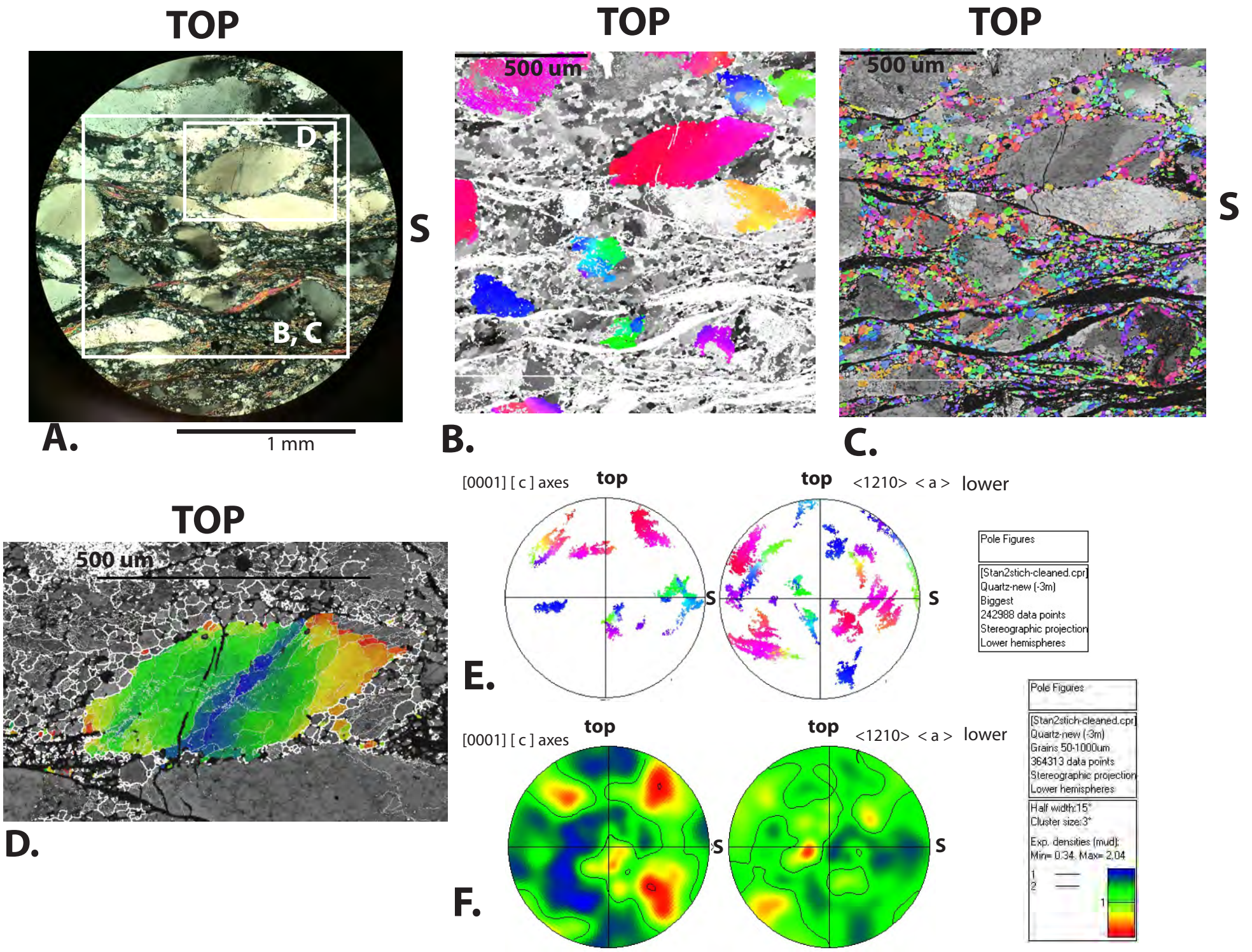

Figure SA2. Photomicrographs and EBSD data for part of oriented thin section from sample ELM06 WR-41. A. Photomicrograph (crossed polarized light) of area imaged showing large detrital quartz grains mantled by fine-grained, dynamically recrystallized quartz in a matrix consisting of mica and quartz-rich bands. For location of A see Figure SA1A. B. and C. EBSD Band contrast + Euler angle maps at ~1 μm resolution based upon ~ 0.5 million indexed points highlighting in color. Big quartz grains > 1000 μm in B. and small grains between 50-1000 μm in C. Grains smaller than 50 μm were removed because these can be artifacts of the measurement process. Undulatory extinction and subgrain development can be seen in large quartz grains while the smaller quartz grains are mostly equant. D. Band contrast + Euler angle map of one large quartz grain (red grain in B). Colors indicate misorientation of crystallographic axes with respect to central point in grain (crosshairs); maximum misorientation (indicated by red) is 20° from the central point. Subgrain boundaries that are defined by misorientations of <1° are shown by thin white lines. Grain boundaries defined by misorientations of >15° are shown by thick white lines. The large grain shows progressive and smoothly varying misorientation away from the grain core toward both grain tips suggesting misorientation by dislocation glide. The small grains around this quartz porphyroclast are separated from the porphyroclast by misorientations of >15°, suggesting that they are not related to each other by the process of subgrain rotation. E. Lattice preferred orientation of the large grains (the colors in the LPO and the map (Fig. SA2B) match). Lattice rotations within individual grains are easy to see. F. Contoured crystallographic orientations of small grains (50-1000 μm) only.

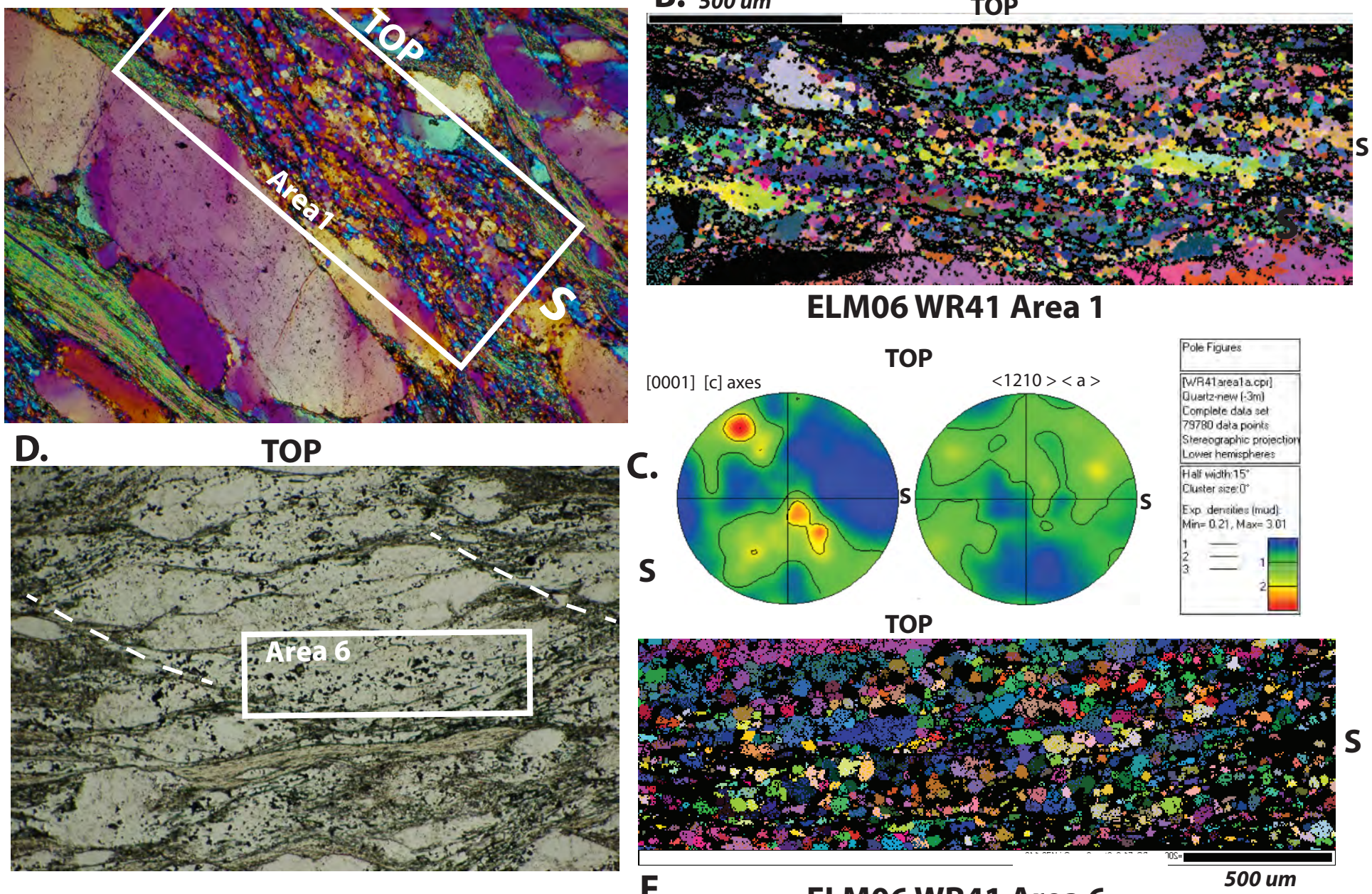

Figure SA3. EBSD data from small sub areas, Area 1 and Area 6, sample ELM06 WR-41. For locations, see Figure SA1A. A. Photomicrograph of Area 1 (crossed polarized light with gypsum plate in) showing analysis area surrounded by box. B. Band contrast + Euler angle map of quartz grains in Area 1. C. Contoured pole figure diagrams for quartz grains imaged and analyzed in B. D. Photomicrograph (plain light) and E. (crossed polarized light with gypsum plate in) of Area 6 showing analysis area surrounded by box. F. Band contrast + Euler angle map of quartz grains in Area 6. G. Contoured pole figure diagrams for quartz grains imaged and analyzed in F. For discussion, see Appendix A text.

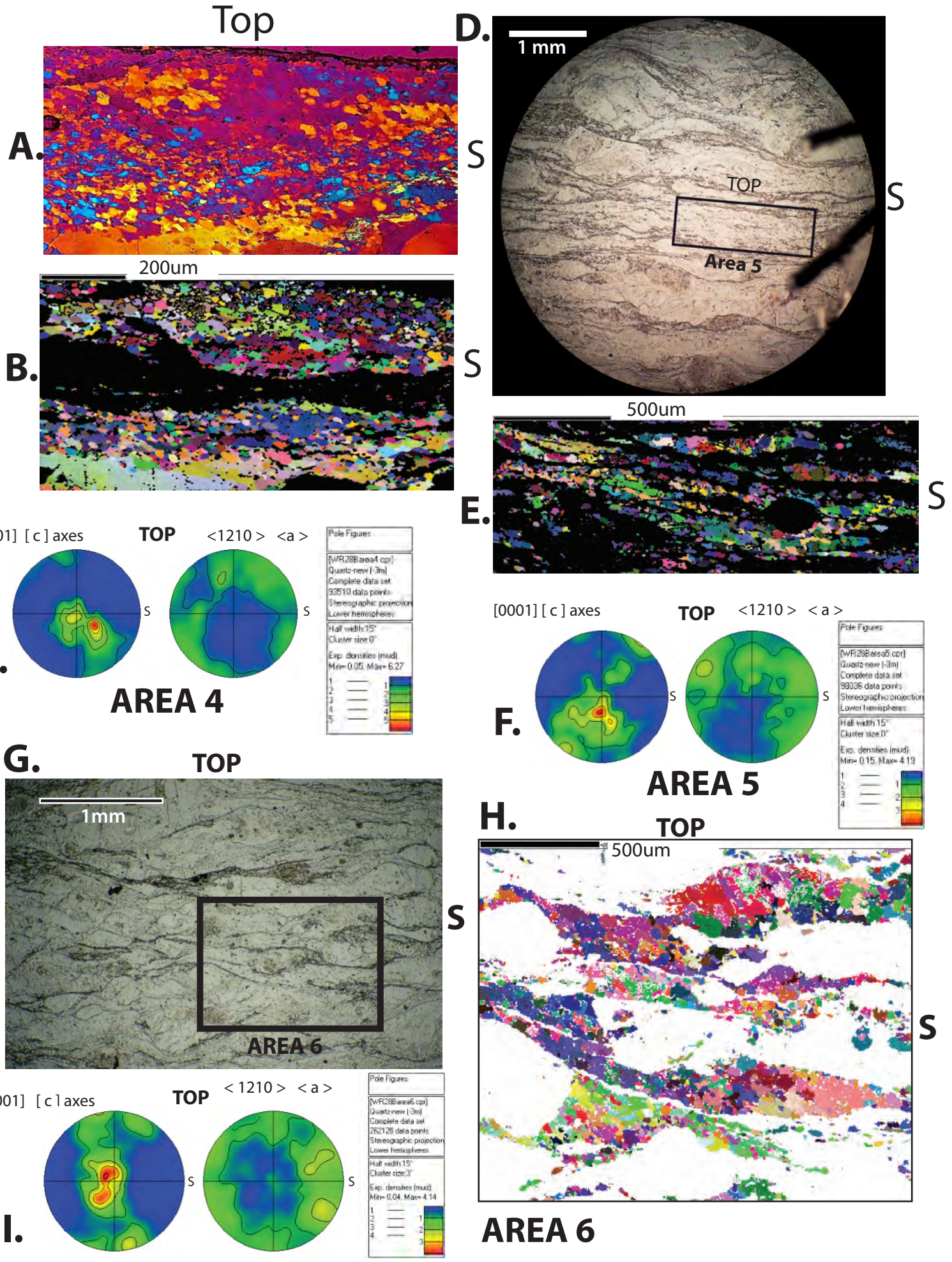

Figure SA4. EBSD data from three small areas of sample ELM06 WR28B. For sample location see Fig. 3. S, South. A. Photomicrograph (crossed polarized light with gypsum plate in) of Area 4, same scale as B. B. Band contrast + Euler angle map of quartz grains in Area 4. Band of black material is albite, which was not indexed. C. Contoured pole figure diagrams for orientations of quartz grains imaged and analyzed in B. D. Photomicrograph (plane light) of area 5, showing analysis area in box. This larger-scale photomicrograph illustrates the rotation of rigid feldspar grains in a more deformable and quartz-rich matrix. E. Band contrast + Euler angle map of quartz grains in Area 5. Black areas are feldspar and mica, which were not indexed. F. Contoured pole figure diagrams for quartz grains imaged and analyzed in E. G. Photomicrograph (plane light) of area 6 analysis in box. Rotation of rigid feldspars is also clear in this photomicrograph, with shear bands around them dipping both N and S. H. Band contrast + Euler angle map of quartz grains in Area 6 (colored) and feldspar (white), which was not indexed. I. Contoured pole figure diagrams for quartz grains imaged and analyzed in H. For discussion, see text of Appendix SA.